



# Wind-capture-accelerate device for performance improvement of vertical-axis wind turbines: External diffuser system

Limin Kuang <sup>a</sup>, Jie Su <sup>a</sup>, Yaoran Chen <sup>a</sup>, Zhaolong Han <sup>a, b, c, d, e</sup>, Dai Zhou <sup>a, b, c, d, \*</sup>, Kai Zhang <sup>f</sup>, Yongsheng Zhao <sup>a, b</sup>, Yan Bao <sup>a, b, c</sup>

<sup>a</sup> School of Naval Architecture, Ocean and Civil Engineering, Shanghai Jiao Tong University, Shanghai, 200240, China

<sup>b</sup> State Key Laboratory of Ocean Engineering, Shanghai Jiao Tong University, Shanghai, 200240, China

<sup>c</sup> Shanghai Key Laboratory for Digital Maintenance of Buildings and Infrastructure, Shanghai Jiao Tong University, Shanghai, 200240, China

<sup>d</sup> Key Laboratory of Hydrodynamics of Ministry of Education, Shanghai Jiao Tong University, Shanghai, 200240, China

<sup>e</sup> Institute of Polar and Ocean Technology, Institute of Marine Equipment, Shanghai Jiao Tong University, Shanghai, 200240, China

<sup>f</sup> Department of Mechanical and Aerospace Engineering, Rutgers University, Piscataway, NJ, 08854, USA

## ARTICLE INFO

### Article history:

Received 30 March 2021

Received in revised form

30 August 2021

Accepted 25 September 2021

Available online 28 September 2021

### Keywords:

Vertical-axis wind turbine

External diffuser system

Power performance

Parametric analysis

Improved delayed detached-eddy simulation

## ABSTRACT

The unsatisfactory power performance hinders the development of vertical-axis wind turbines (VAWTs). Installing a wind-capture-accelerate device outside the VAWT is one possible way to alleviate this situation. In the current study, an external diffuser system is designed to improve the power performance of the VAWT. The three-dimensional improved delayed detached-eddy simulation is employed to predict the aerodynamics. First, the power performance and aerodynamic loads of the VAWT equipped with different types of basic diffusers are compared at the optimal tip speed ratio (TSR) of 1.5. Then, a stepwise parametric analysis of the effects of size parameters, i.e., projected length,  $1 \leq L_1/D \leq 2.5$  and diffusion angle,  $10^\circ \leq \theta_1 \leq 30^\circ$ , is performed in various operating conditions, i.e.,  $0.4 \leq \text{TSR} \leq 2.5$ . Afterwards, the effects of the rear flange and anterior ejector on the behaviors of the basic diffuser are investigated, and the flow structures around the VAWT are analyzed. Finally, an application prospect evaluation of the system is conducted. The results show that the enclosed type basic diffuser with curved inner surface can significantly improve the power performance of the VAWT at moderate and high TSRs. The aerodynamic loads on the blade are enlarged and present more fluctuations. The power coefficient of the VAWT at  $\text{TSR} = 1.5$  is increased by 51.73% when  $L_1/D = 2$  and  $\theta_1 = 20^\circ$ . The flange and ejector can further enhance the capability of the basic diffuser by increasing the pressure difference and stabilizing the flow field. It is concluded that the external diffuser system would have potential applications in specific urban areas.

© 2021 Elsevier Ltd. All rights reserved.

## 1. Introduction

With the continuous depletion of fossil fuels and the growing concern about environmental pollution, the utilization of renewable and clean energy has become an important issue for the sustainable society [1,2]. Wind energy is widely distributed in urban and offshore areas, and rapid progress has been made in wind power generation over the past few decades. As the two main tools for wind energy conversion, the horizontal-axis wind turbine (HAWT) and the vertical-axis wind turbine (VAWT) are distinguished by the direction of the rotation axis [3,4]. Although the

HAWT currently dominates the commercial wind turbine market, small and medium-sized VAWTs are gaining increasing attention because of their simple structures and low costs [5,6]. However, the unsatisfactory power performance hinders the development of the VAWT [7]. One of the main reasons is that the aerodynamics of the VAWT present more complex characteristics than those of the HAWT due to the large variation in the angle of attack (AOA) during the rotation [8,9]. Therefore, it is important to solve the aerodynamic problems of the VAWT and improve its power performance.

To achieve this goal, a variety of methods have been developed to predict the aerodynamics of the VAWT, which can be broadly classified into three categories, i.e., experimental methods, analytical modeling methods, and computational fluid dynamics (CFD) methods [5]. Although the experimental methods

\* Corresponding author. School of Naval Architecture, Ocean and Civil Engineering, Shanghai Jiao Tong University, Shanghai, 200240, China.

E-mail address: [zhoudai@sjtu.edu.cn](mailto:zhoudai@sjtu.edu.cn) (D. Zhou).

represented by the wind tunnel test can give the most accurate results, considering their high construction costs, the latter two methods are more widely employed in academia and industry. Due to the limitation of the computing resources, the analytical modeling methods including the streamtube approach, vortex approach, and cascade approach have been extensively applied to the study of the VAWT. The basic idea of these efficient low-fidelity approaches is to simplify the prediction process of the rotor aerodynamics using the momentum theory, potential flow theory, and cascade theory [10]. To date, a number of advanced analytical modeling methods have been proposed based on the pioneering researches of Templin et al. [11], Paraschivoiu et al. [12], Strickland et al. [13], and Hirsch et al. [14], such as the improved double-multiple streamtube approach [15], vortex panel model [16], and low-order model [17], which significantly improve the computational accuracy. However, some critical flow information (e.g., vortical structures) cannot be obtained from these methods, thereby restricting the further investigations of the aerodynamic problems.

In recent years, the CFD methods have gained wide popularity because of their high fidelity, powerful access to the flow information, and the rapid development of the computing resources [18,19]. Many researchers have contributed their efforts to explore the aerodynamics of the VAWT in different operating conditions through the CFD methods. Rezaeih et al. [20] investigated the impact of the tip speed ratio (TSR) on the aerodynamic performance of a two-straight-bladed VAWT using the unsteady Reynolds-Averaged Navier-Stokes (URANS) approach. The results showed that the decreased TSR would lead to strong fluctuations in the aerodynamic loads and promote the laminar-to-turbulent transition on the blade. Peng and Lam [21] employed the three-dimensional large-eddy simulation (LES) to analyze the aerodynamic performance of a five-straight-bladed VAWT in the turbulent flow. It was found that a moderate degree of turbulence was beneficial to the aerodynamics of the blade, which energized the boundary-layer flow and delayed the dynamic stall. Hand et al. [22] studied the aerodynamics of a single airfoil in Darrieus motion with the help of the URANS approach. They observed that high Reynolds numbers could reduce the unstable responses of the aerodynamic parameters of the airfoil (e.g., torque coefficient) and alleviate the negative effects of the dynamic stall.

As numerous studies provided supports for solving the aerodynamic problems of the VAWT, three categories of approaches were summarized to improve its power performance, i.e., adopting efficient blade configurations, developing novel rotor structures, and installing wind-capture-accelerate devices or deflectors outside the rotor [23]. Most researchers focused on the first approach and a series of new blades were invented, including the leading edge-slotted [9], leading edge-serrated [24], V-shaped [19], winglet-attached [18,25], and Gurney flap-attached [26,27]. These configurations can improve the power performance of the VAWT by changing the flow structures around the blade, e.g., suppressing the flow separation. However, the existing manufacturing process may not meet the demands of some blades, thereby restricting their current applications. For the second approach, Liu et al. [28] placed a modified Savonius rotor inside a three-straight-bladed VAWT and simulated its aerodynamics. The results showed that this hybrid VAWT has excellent self-starting performance. Poguluri et al. [29] proposed a co-axial contra-rotating VAWT and demonstrated its superiority in reducing the cyclic loading at the shaft base. Villeneuve et al. [30] found that a well-designed support structure with rounded blade-strut joints is beneficial to the rotor aerodynamics. However, the improvement of these novel rotor structures on the power performance of the VAWT is not as pronounced as that of the first approach, which needs further

investigations. Therefore, the third approach is considered in the current study and a diffuser-based wind-capture-accelerate device is designed.

The concept of the diffuser for wind turbines was proposed by Gilbert et al. [31] and Foreman et al. [32]. As an external ducted device capable of concentrating the unidirectional flow, its basic idea is to improve the power performance of the wind turbine by enlarging the local wind velocity. Subsequent researchers experimentally demonstrated the capability of the diffuser to capture and accelerate the wind [33], and have made preliminary attempts to apply it to wind turbines, e.g., shrouded wind turbines [34,35]. However, this topic fell into silence from the 1990s and did not receive renewed attention until 2008, when the application of the flanged diffuser on a medium-sized HAWT was systematically investigated in the research of Ohya et al. [36]. It was shown that the diffuser was able to increase the power output of the HAWT by a factor of about 4–5. Since then, several studies have successively analyzed the effects of different size parameters on the behaviors of the diffuser to further enhance its capability while preparing it for commercial applications on the HAWT [37–41].

Considering the outstanding benefits of the diffuser, it seems to be a good choice to equip it on the relatively underperforming VAWT. However, only a few researchers have used this technology to improve the power performance of the VAWT. Hashem et al. [42] investigated the effects of the flanged diffuser on the power output of a three-straight-bladed VAWT using two-dimensional CFD simulations. It was found that the diffuser had a considerable benefit on the VAWT, increasing its power coefficient by a factor of about 3.9. On this basis, a stepwise parametric analysis of the effects of size parameters of the diffuser was performed by Dessoky et al. [43], and the aerodynamic noise of a two-straight-bladed VAWT with and without the diffuser was compared. The results showed that the optimized diffuser could increase the power coefficient of the VAWT by 82%, but would generate more noise. The experiments conducted by Watanabe et al. [44] and Wang et al. [45] also demonstrated the potential feasibility of applying the diffuser to the VAWT.

Although the aforementioned studies have explored the application of the diffuser on the VAWT from various aspects, there is still more space for the design of the diffuser-based devices. The limitations of the existing studies and the issues that need to be addressed are as follows:

- (1) The basic diffuser can be evolved into a more effective form by installing additional components (e.g., rear flange and anterior ejector), but its evolutionary stages have not yet been systematically modeled from a three-dimensional perspective.
- (2) Choosing a promising type of basic diffuser is important for the subsequent design. However, the different types of basic diffusers have not yet been comprehensively compared.
- (3) Two-dimensional numerical modeling tends to overestimate the power performance of the VAWT with low aspect ratio due to the neglect of the blade tip vortices [46]. This inherent deficiency may affect the reliability of the parametric analysis.
- (4) Most of the existing studies focused on the variation of the power coefficient of the VAWT, while the aerodynamic loads on the blade and the flow structures around the rotor were rarely analyzed. However, such information is essential for understanding the working mechanisms of the diffuser-based devices.
- (5) Given that there are some doubts about applying the diffuser to the VAWT, it is necessary to evaluate the application prospects of such devices.

Therefore, the current study aims to overcome these limitations by designing and modeling an external diffuser system with three evolutionary stages. The three-dimensional improved delayed detached-eddy simulation (IDDES) is employed to address the numerical issues.

It should be noted that the main doubt of applying the diffuser to the VAWT is that the omnidirectionality of the rotor may be compromised. Admittedly, concentrating only the unidirectional flow is the biggest deficiency of the diffuser. However, the corresponding negative effect would be alleviated when the VAWT is located in specific environments with a dominant wind direction, e.g., compact urban areas. Some suitable solutions have been proposed for the placement of the VAWT equipped with a diffuser (cowling), i.e., installed between the buildings [47,48], mounted on the rooftops [49–52], and combined with the wind catchers [53] (see Fig. 1). These potential application scenarios undoubtedly give the authors confidence. Besides, the external diffuser system designed in the current study also has a certain passive yaw capability, which will be presented in the subsequent sections.

The rest of the current study is organized as follows: The geometric models of the VAWT and external diffuser system are presented in Section 2. The numerical method including the IDDES, computational domain, mesh topology, and solver settings are described in Section 3. The mesh independence test and solution validation are conducted in Section 4. Section 5 presents the comparison of different types of basic diffusers, parametric analysis of the effects of size parameters, investigation of the effects of flange and ejector, analysis of the flow structures, and application prospect evaluation of the system. The concluding remarks are provided in Section 6.

## 2. Geometric model

### 2.1. Vertical-axis wind turbine

Without loss of generality, a conventional small-sized three-straight-bladed VAWT designed by Elkhoury et al. [54] is selected as the main research objective of the current study. The schematic diagram and geometric properties of the VAWT are presented in Fig. 2 and Table 1, respectively. The struts are neglected because they have small influence on the numerical prediction of the aerodynamics [55].

The aerodynamic parameters of the blade during the rotation are illustrated in Fig. 3. To simplify the performance analysis of the VAWT, the induced velocity is neglected in the calculation of the

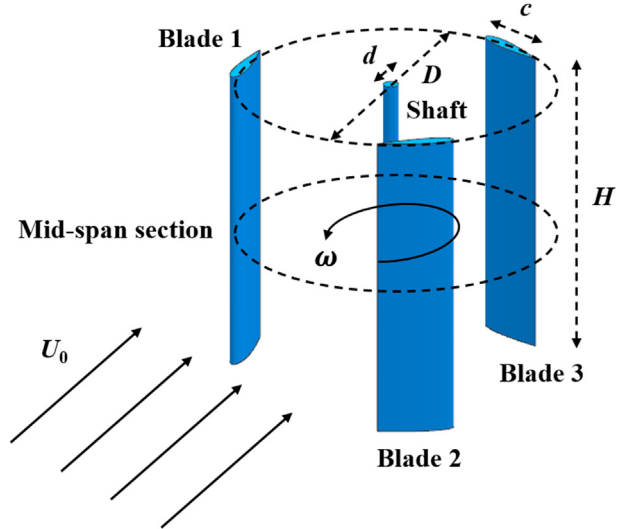


**Fig. 2.** Schematic diagram of the selected VAWT.

**Table 1**

Geometric properties of the selected VAWT.

Property	Symbol	Value
Airfoil	—	NACA 0018
Span length	H	0.800 m
Chord length	c	0.200 m
Shaft diameter	d	0.050 m
Rotor diameter	D	0.800 m

relative velocity  $U_{rel}$  of the blade [19,20,24]:

$$\overrightarrow{U_{rel}} = \overrightarrow{R} \times \overrightarrow{\omega} + \overrightarrow{U_0} \quad (1)$$

$$U_{rel} = U_0 \sqrt{TSR^2 + 2TSR\cos\theta + 1} \quad (2)$$

where  $R$ ,  $\omega$ ,  $U_0$ , and  $\theta$  are the rotor radius, angular velocity, inflow velocity, and azimuthal angle, respectively.

The TSR is defined as:

$$TSR = \frac{\omega D}{2U_0} \quad (3)$$

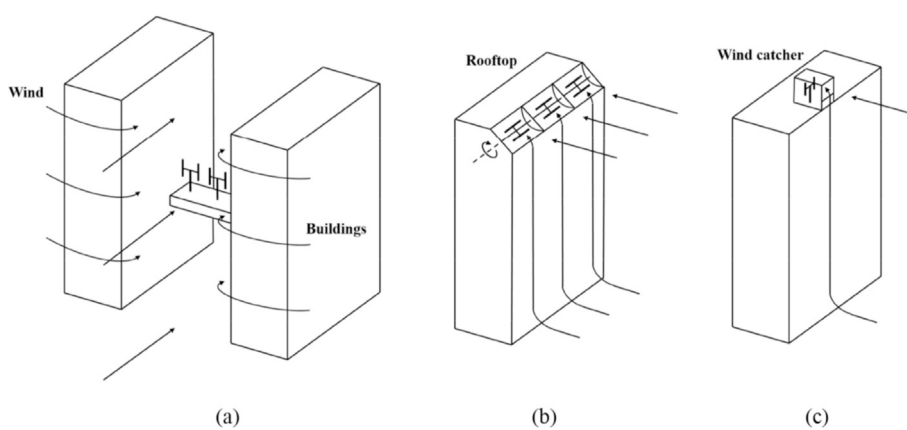


**Fig. 1.** Schematic diagram of the VAWTs located in specific urban areas (not to scale): (a) installed between the buildings; (b) mounted on the rooftops (Crossflex concept [49]); (c) combined with the wind catchers.

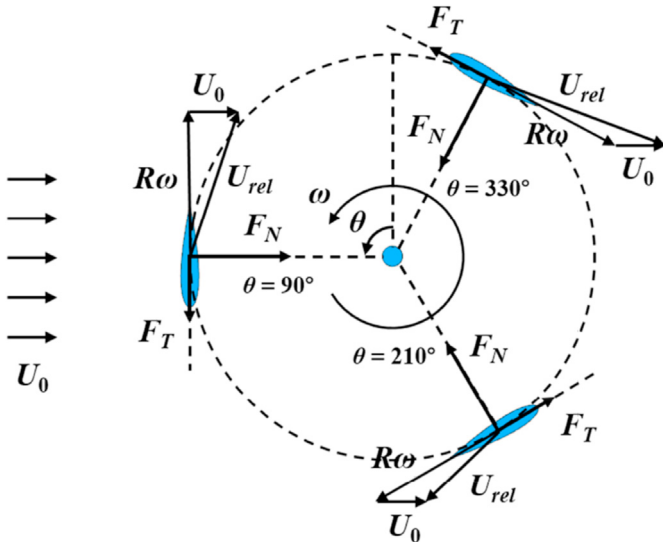


**Fig. 3.** Schematic diagram of the aerodynamic parameters of the blade.

The tangential force coefficient  $C_T$  and normal force coefficient  $C_N$  of the blade can be calculated as follows:

$$C_T = \frac{F_T}{\rho U_{rel}^2 c H / 2} \quad (4)$$

$$C_N = \frac{F_N}{\rho U_{rel}^2 c H / 2} \quad (5)$$

where  $F_T$ ,  $F_N$ , and  $\rho$  are the tangential force, normal force, and air density, respectively.

The power coefficient  $C_p$ , torque coefficient  $C_Q$ , and thrust coefficient  $C_{thrust}$  of the VAWT can be calculated as follows:

$$C_p = \frac{Q \omega}{\rho U_0^2 H D / 2} \quad (6)$$

$$C_Q = \frac{Q}{\rho U_0^2 H D^2 / 4} \quad (7)$$

$$C_{thrust} = \frac{F_{thrust}}{\rho U_0^2 H D / 2} \quad (8)$$

where  $Q$  and  $F_{thrust}$  are the torque and thrust, respectively. The direction of  $F_{thrust}$  is consistent with the streamwise direction.

## 2.2. External diffuser system

The geometric model of the external diffuser system is presented in Fig. 4. The basic diffuser, rear flange, and anterior ejector constitute the three evolutionary stages of the system (i.e., stage 1: basic diffuser; stage 2: basic diffuser with flange, also known as the flanged diffuser; stage 3: basic diffuser with flange and ejector). As

shown in Fig. 5, four types of basic diffusers are considered at stage 1, and the main difference between them is whether they are enclosed and whether their inner surfaces are curved. The size parameters of the system include the inlet diameter  $D_{inlet1}$ , outlet diameter ( $D_{outlet1}$ ,  $D_{outlet2}$ , and  $D_{outlet3}$ ), projected length ( $L_1$ ,  $L_{2-1}$ ,  $L_{2-2}$ , and  $L_3$ ), and diffusion angle ( $\theta_1$ ,  $\theta_2$ , and  $\theta_3$ ). The mathematical relationships between them are expressed as follows:

$$D_{outlet1} = D_{inlet1} + 2L_1 \tan \theta_1 \quad (9)$$

$$D_{outlet2} = D_{outlet1} + 2L_{2-1} \quad (10)$$

$$D_{outlet3} = D_{inlet1} + 2L_3 \tan \theta_3 \quad (11)$$

$$L_{2-2} = L_{2-1} \tan \theta_2 \quad (12)$$

Based on the geometric properties of the selected VAWT, the initial size parameters of the system are listed in Table 2. Without moving the location of the rotor, the comparison of different types of basic diffusers, parametric analysis of the effects of size parameters, and investigation of the effects of flange and ejector are presented in Section 5.

## 3. Numerical method

### 3.1. Improved delayed detached-eddy simulation

The commercial computer-aided engineering (CAE) software STAR-CCM+ version 13.04 is utilized as the CFD solver in the current study. The three-dimensional IDDES is employed to handle the incompressible Navier-Stokes equations. As a balanced and powerful hybrid RANS/LES approach, the IDDES solves the problem of log-layer mismatch in DES by providing some wall-modeled LES (WMLES) capabilities to the DDES [56]. On the one hand, a new definition of the subgrid length-scale  $\Delta$  in LES that considers both the grid spacing and wall distance was given, expressed as [56]:

$$\Delta = \min \{ \max \{ 0.15 d_w, 0.15 h_{max}, h_{wn} \}, h_{max} \} \quad (13)$$

where  $d_w$ ,  $h_{max}$ , and  $h_{wn}$  are the distance to the wall, maximum grid spacing, and grid spacing in the wall-normal direction, respectively. On the other hand, a new numerical strategy that could seamlessly switch between the DDES and WMLES depending on the inflow condition and grid resolution was proposed. The length-scales of the DDES, WMLES, and IDDES are defined as follows [56]:

$$l_{DDES} = f_d l_{RANS} - f_d \max \{ 0, (l_{RANS} - l_{LES}) \} \quad (14)$$

$$l_{WMLES} = f_B (1 + f_e) l_{RANS} + (1 - f_B) l_{LES} \quad (15)$$

$$l_{IDDES} = \max \{ (1 - f_d) f_B \} (1 + f_e) l_{RANS} + (1 - \max \{ (1 - f_d) f_B \}) \times l_{LES} \quad (16)$$

where  $f_d$ ,  $f_B$ , and  $f_e$  are empirical blending functions.  $l_{RANS}$  and  $l_{LES}$  are the length-scales of the RANS approach and LES, respectively.

Based on the above modifications, the IDDES not only inherits the advantages of DES and DDES, such as higher accuracy compared with the RANS approach and lower cost compared with LES, but

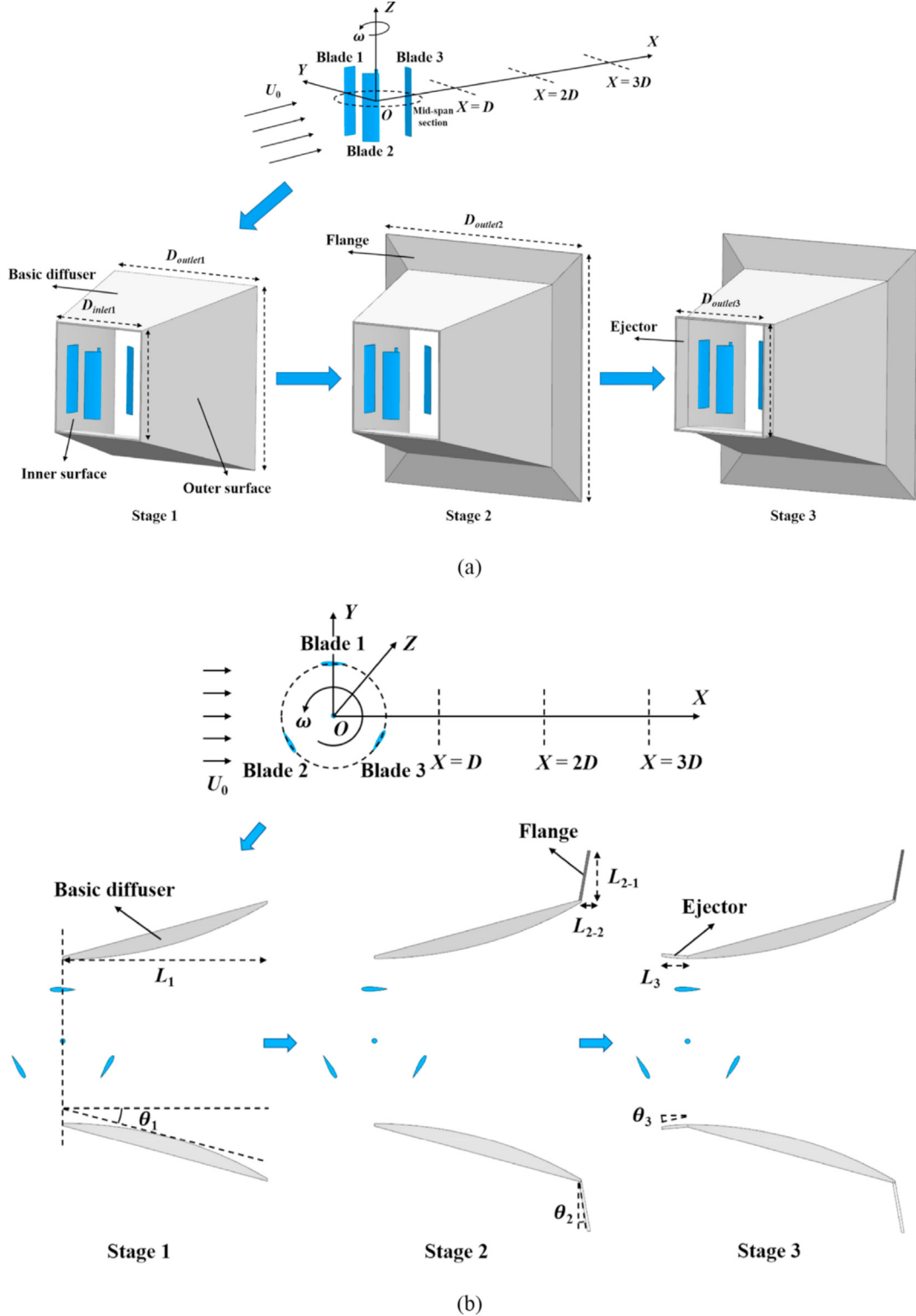


**Fig. 4.** Geometric model of the external diffuser system: (a) three-dimensional view; (b) vertical view (mid-span section).

also performs better in simulating the attached and separated flow at high Reynolds numbers [56]. In the authors' previous studies [55,57,58], the IDDES with the background of the SST  $k-\omega$  turbulence model has also shown good results in predicting the aerodynamics of the VAWT.

### 3.2. Computational domain and mesh topology

As shown in Fig. 6, a cuboid computational domain is constructed to perform the simulations. To avoid the flow acceleration caused by the large blockage ratio [59], the length  $L$ , width  $W$ , and

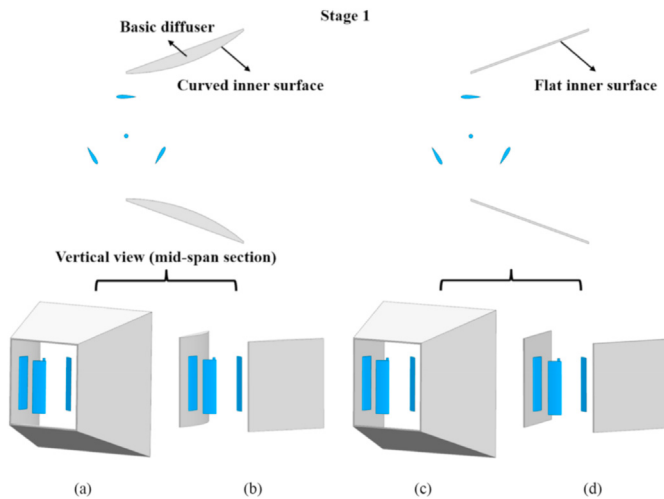


**Fig. 5.** Schematic diagram of different types of basic diffusers: (a) enclosed type with curved inner surface; (b) open type with curved inner surface; (c) enclosed type with flat inner surface; (d) open type with flat inner surface.

**Table 2**  
Initial size parameters of the external diffuser system.

Parameter	Symbol	Value
Inlet diameter	$D_{inlet1}$	$1.6D$
Outlet diameter	$D_{outlet1}$	$2.7D$
	$D_{outlet2}$	$3.7D$
Projected length	$D_{outlet3}$	$1.7D$
	$L_1$	$1.5D$
	$L_{2-1}$	$0.5D$
	$L_{2-2}$	$0.13D$
	$L_3$	$0.5D$

$$W = \begin{cases} 12D & \text{No diffuser} \\ 12D_{outlet1} & \text{Stage 1} \\ 12D_{outlet2} & \text{Stage 2, Stage 3} \end{cases} \quad (18)$$

$$E = \begin{cases} 12D & \text{No diffuser} \\ 12D_{outlet1} & \text{Stage 1} \\ 12D_{outlet2} & \text{Stage 2, Stage 3} \end{cases} \quad (19)$$

The domain consists of two parts: One cylindrical rotational region and one fixed background region. The contact surfaces between these two regions are defined as the interfaces, where the physical information is transferred through the sliding mesh technique. The VAWT is located in the rotational region and can rotate at a preset angular velocity. According to the CFD guidelines for VAWTs [59,60], the diameter and height of the rotational region are set to  $1.5D$  and  $1.5H$ , respectively. The inlet and outlet of the domain are set as the velocity inlet ( $U_0 = 8.0$  m/s) and pressure outlet ( $P_0 = 0.0$  Pa), respectively. The remaining boundaries are in symmetric conditions to avoid the reflection effect [24]. The surfaces of the VAWT and external diffuser system are set as the no-slip walls. For the specification of the turbulence values, the turbulence intensity, turbulent viscosity ratio, and turbulent velocity scale are set to 0.8%, 10, and 1 m/s, respectively.

As shown in Fig. 7, the trimmed grid mesher is employed to generate the mesh topology. To accurately predict the aerodynamics of the VAWT, a mesh refinement is conducted in the rotational region. The prismatic boundary-layer grids are set around the VAWT and external diffuser system to capture the near-wall flow. Taking the case of the blade as an example, the chord-based Reynolds number in the current study is about  $1.53 \times 10^5$ – $3.83 \times 10^5$ . Therefore, based on the authors' previous studies [55,57,58], the growth ratio, number of layers, and total thickness of the boundary-layer grids around the blade are set to

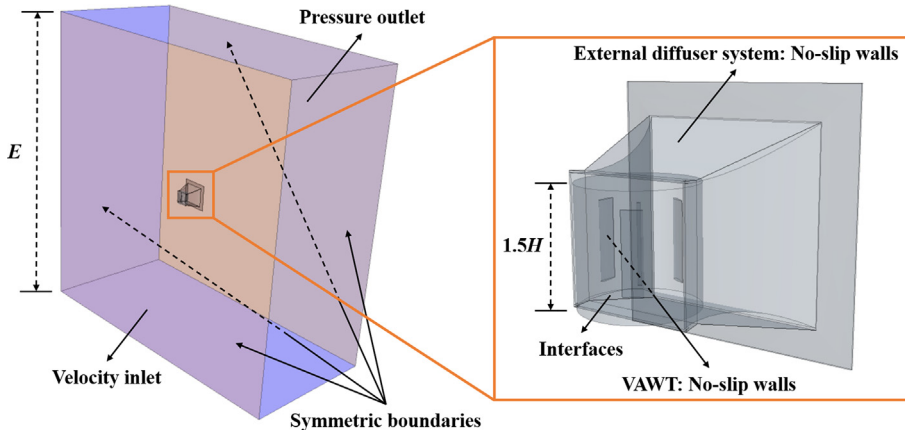


**Fig. 6.** Schematic diagram of the computational domain: (a) three-dimensional view; (b) plan layout (not to scale).

height  $E$  of the domain are set as follows:

$$L = 20D \quad \text{All the conditions} \quad (17)$$

1.2, 26, and 0.006 m, respectively, to meet the requirement of IDDES for  $y^+ < 1$ . The quality of the mesh topology is automatically diagnosed in STAR-CCM+. Taking one of the cases at stage 3 as an example, the overall face validity is equal to 1.00, 99.78% of the grids have a volume change between 0.10 and 1.00, and the

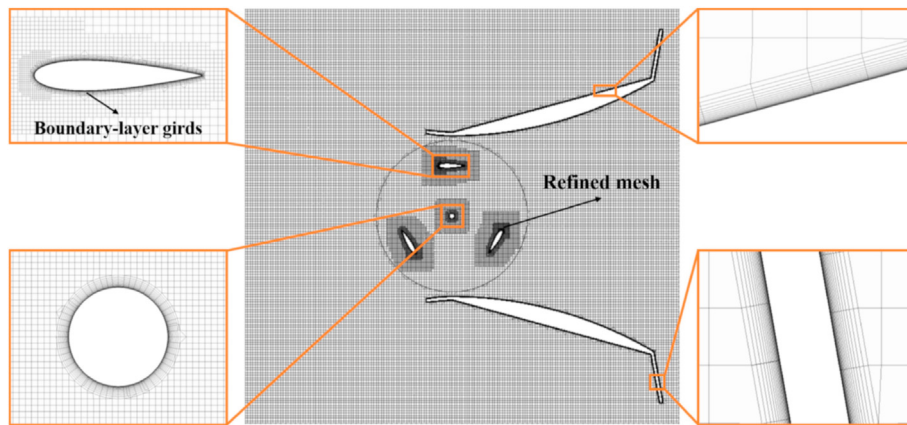


Fig. 7. Schematic diagram of the mesh topology.

maximum grid skewness angle is less than 85°.

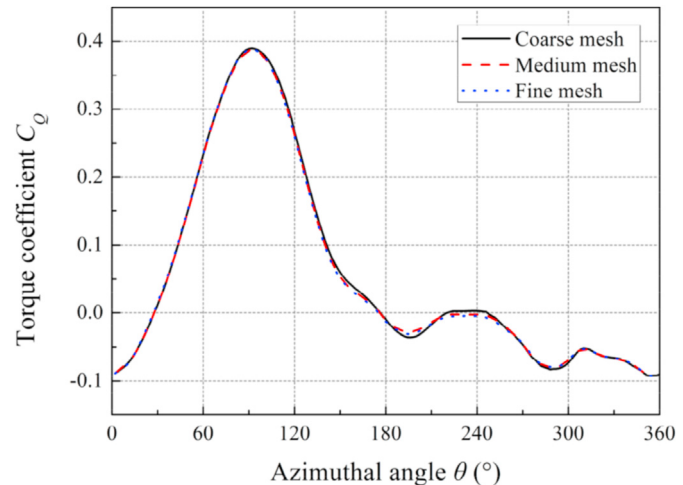
### 3.3. Solver settings

The segregated flow solver with the implicit unsteady approach is employed to perform the transient analysis. The hybrid second-order upwind/bounded central-differencing scheme is adopted to discretize the convection and diffusion terms. The pressure-velocity coupling is realized through the SIMPLE algorithm. For the temporal resolution, an azimuthal increment of 2° is selected in the current study, corresponding to a time step of  $T/180$ , where  $T$  is the period of one turbine revolution. 20 internal iterations are set for each time step to obtain the convergence results after 20 turbine revolutions. The above settings bring the averaged convective Courant number below 1 in most of the rotational region and on the order of 1 around the blades. A detailed sensitivity test of the azimuthal increment is provided in [Appendix A](#).

## 4. Verification and validation

### 4.1. Mesh independence test

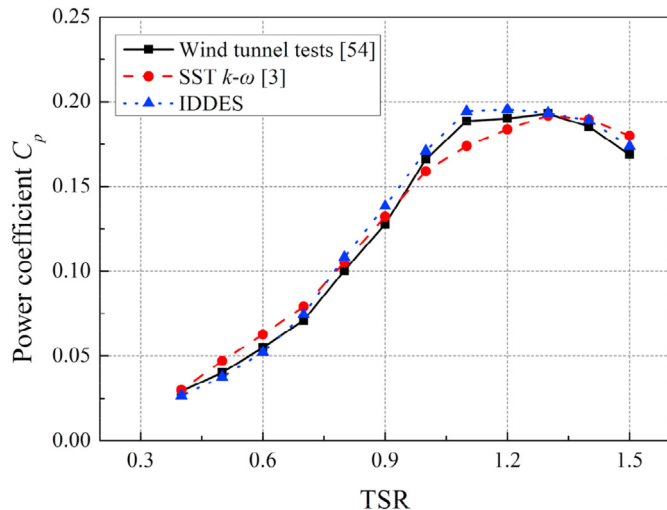
In the current study, a mesh independence test is conducted for the selected VAWT with the basic diffuser (stage 1, enclosed type with curved inner surface, see [Fig. 5](#)). The size parameters of the basic diffuser are set according to [Table 2](#). Three uniformly refined mesh topologies, namely the coarse mesh, medium mesh, and fine mesh, are generated and compared (see [Table 3](#)). The criterion to adjust the number of grids is successively refining the trimmed grid size with a refinement ratio of 1.25 for each coordinate direction. The grid convergence index (GCI) proposed by Roache [61,62], is adopted to provide a consistent manner in reporting the results of the mesh independence test. The GCI is calculated in terms of the averaged power coefficient  $C_p$  of the VAWT at  $TSR = 1.5$  (optimal

Fig. 8. Comparison of the instantaneous torque coefficients of blade 1 predicted by different mesh topologies. ( $TSR = 1.5$ ).

when equipped with the basic diffuser), using a safety factor of 1.25. The values of  $GCI^{fine}$  for the coarse-medium mesh pair and medium-fine mesh pair are  $13.96 \times 10^{-3}$  and  $5.37 \times 10^{-3}$ , respectively, which indicates that the solution has converged with the refinement from the coarse mesh to the fine mesh. Besides, the averaged  $y^+$  on blade 1 for different mesh topologies is around 1 and decreases gradually from the coarse mesh to the fine mesh, which is consistent with the findings of Rezaeih et al. [59]. [Fig. 8](#) depicts the instantaneous torque coefficients  $C_Q$  of blade 1 with respect to the azimuthal angle  $\theta$  for different mesh topologies. It can be seen that the results of the medium mesh and fine mesh are almost identical, and the variation trend of  $C_Q$  predicted by the coarse mesh shows a small deviation. Therefore, in consideration of

**Table 3**  
Comparison of different mesh topologies.

Mesh topology	Total number of grids	Number in rotational region	Number in background region	Predicted power coefficient $C_p$ at $TSR = 1.5$	Averaged $y^+$ on blade 1 at $TSR = 1.5$
Coarse mesh	6,131,104	2,828,068	3,303,036	0.2503	1.118
Medium mesh	10,162,632	4,016,058	6,146,574	0.2462	1.070
Fine mesh	17,305,661	5,881,414	11,424,247	0.2445	1.062



**Fig. 9.** Comparison of the averaged power coefficients of the VAWT predicted by the IDDES with the experimental and numerical data [3,54].

the mesh independence and computational efficiency, the medium mesh is selected for the rest of the simulations.

#### 4.2. Solution validation

To ensure the reliability of the numerical method employed in the current study, a solution validation of the IDDES is conducted. Due to the lack of experimental data for the selected VAWT with the external diffuser system, only the individual VAWT is considered as the research objective. The results of the IDDES are compared with the experimental data extracted from the wind tunnel tests conducted by Elkhoury et al. [54] and the numerical data simulated by Ma et al. [3] using the SST  $k-\omega$  turbulence model. The boundary conditions of the computational domain are set according to the experimental environment (see Section 3.2). The averaged power coefficients  $C_p$  of the VAWT at a series of TSRs are selected as the comparison objectives. It can be seen from Fig. 9 that the results of the IDDES are in good agreement with the experimental data and show a slight improvement compared to the numerical data. Nevertheless, some deviations are observed at moderate TSRs, which could be explained as: (1) The geometrical simplification, i.e., neglecting the support arms, could lead to an overestimation of  $C_p$  [20]; (2) The surface roughness of the VAWT and the loss of mechanical energy during the rotation are not considered [20,57]. Overall, the current numerical method can provide reliable predictions of the aerodynamics of the VAWT for the rest of the simulations.

### 5. Results and discussion

#### 5.1. Different types of basic diffusers

This subsection compares the effects of different types of basic diffusers (stage 1, see Fig. 5) on the power performance and aerodynamics loads of the selected VAWT. The size parameters of the basic diffuser are set according to Table 2. Fig. 10 shows the averaged power coefficients  $C_p$  of the VAWT at TSR = 1.5 (optimal when

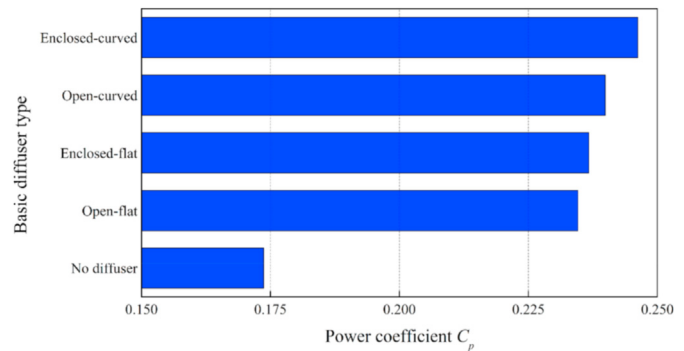


**Fig. 10.** Comparison of the averaged power coefficients of the VAWT for different types of basic diffusers. (TSR = 1.5).

equipped with the basic diffuser). It can be seen that all types of basic diffusers can significantly improve the power performance of the VAWT, especially the enclosed type with curved inner surface, which increases the value of  $C_p$  by 41.74%. The open type with flat inner surface is less effective than the other three types, leading to an increase in  $C_p$  of 35.06%. Moreover, the enclosed type is better than the open type, on which the relatively optimal improvement can be obtained by using the curved inner surface.

Fig. 11(a) depicts the instantaneous torque coefficients  $C_Q$  of blade 1 with respect to the azimuthal angle  $\theta$  (see Fig. 3) at TSR = 1.5. It can be seen that all types of basic diffusers can increase the values of  $C_Q$  in most of the upwind region ( $0^\circ \leq \theta \leq 180^\circ$ ) and lead to a slight decrease of  $C_Q$  in the downwind region ( $180^\circ \leq \theta \leq 360^\circ$ ). The enclosed type with curved inner surface can bring the peak value of  $C_Q$  at  $\theta = 90^\circ$  to the maximum and make  $C_Q$  present more fluctuations in the condition of  $\theta \geq 180^\circ$ . Besides, the difference between the effects of the other three types on  $C_Q$  is small, while the open type with flat inner surface is still relatively inferior, mainly due to its minimal boost to the peak value of  $C_Q$  in the upwind region. Moreover, it should be noted that the overall variation trend of  $C_Q$  will not be changed by the basic diffuser. Fig. 11(b) illustrates the comparison of the instantaneous thrust coefficients  $C_{thrust}$  of blade 1 within one turbine revolution. Unlike the case of  $C_Q$ , the value of  $C_{thrust}$  is increased by the basic diffuser at almost every azimuthal angle, rather than only in the upwind region. For the enclosed type with curved inner surface, the value of  $C_{thrust}$  at  $\theta = 240^\circ$  is 373.08% larger than that of the bare VAWT. This significant enlargement of the thrust in the downwind region ultimately leads to an unstable power output corresponding to the fluctuating power coefficients depicted in Fig. 11(a). The azimuthal angle-varying tangential force coefficients  $C_T$  and normal force coefficients  $C_N$  are depicted in Fig. 11(c) and (d), respectively. It can be seen that all types of basic diffusers change the variation trends of  $C_T$  and  $C_N$ , i.e., the corresponding curves are shifted to the right along the abscissa. Similar to the case of  $C_{thrust}$ , the peak and valley values of  $C_T$  are increased to a certain extent where the enclosed type with curved inner surface contributes the most, providing higher driving force and lower resistance for the rotor rotation, which is beneficial to the self-starting performance of the VAWT. Besides, the presence of lower  $C_N$  in the downwind region indicates that the aerodynamic load on blade 1 in the normal direction is enlarged significantly.

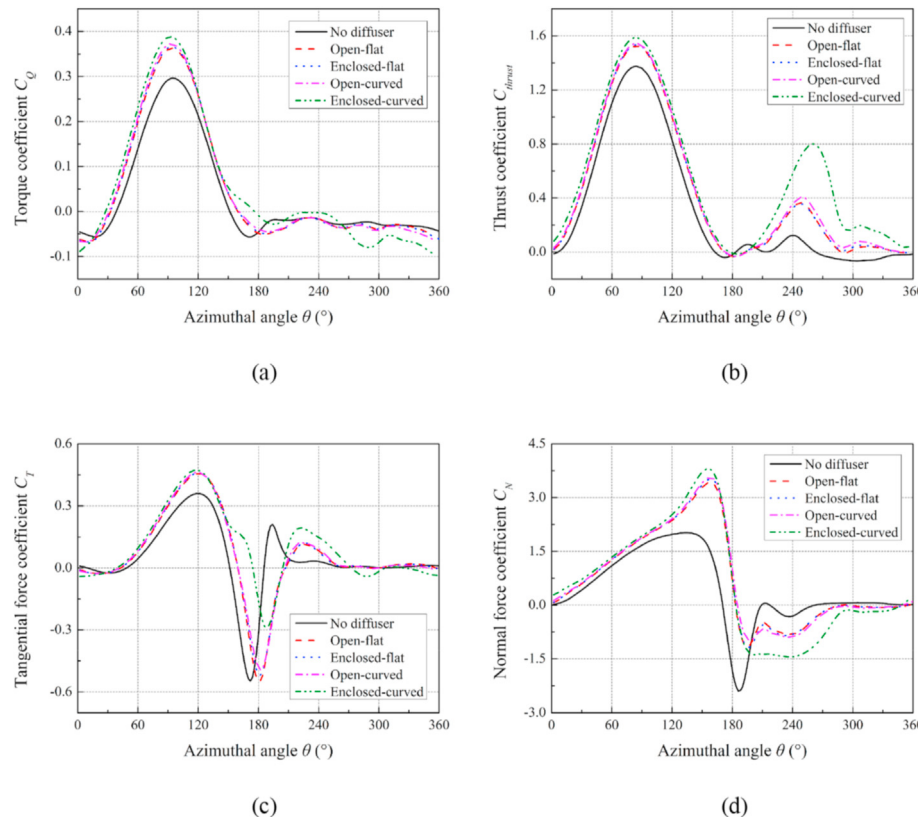


**Fig. 11.** Comparison of the instantaneous force coefficients of blade 1 for different types of basic diffusers: (a) torque coefficient; (b) thrust coefficient; (c) tangential force coefficient; (d) normal force coefficient. (TSR = 1.5).

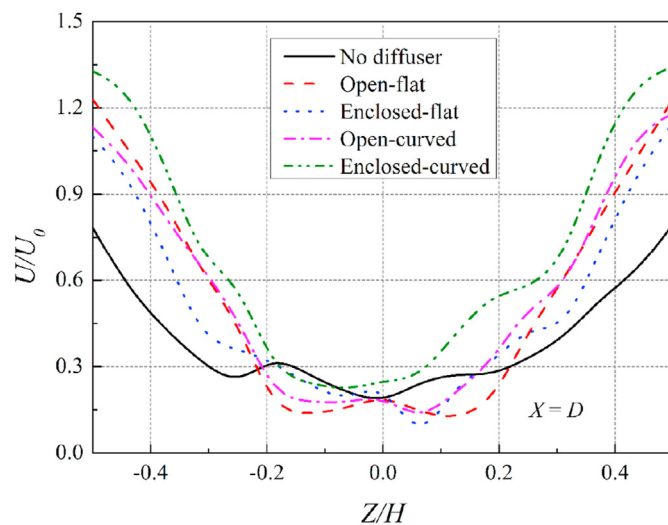


**Fig. 12.** Comparison of the averaged normalized wake profiles of the VAWT in the X-Z plane at the downstream distance of  $X = D$  for different types of basic diffusers. (TSR = 1.5).

To explore the working mechanism of the basic diffuser and to explain the aforementioned physical phenomena, the wake characteristics of the VAWT are investigated. Fig. 12 depicts the averaged normalized wake profiles of the VAWT in the X-Z plane at the downstream distance of  $X = D$  (see Fig. 4(a)). It can be seen that all types of basic diffusers greatly enlarge the flow velocity around the

VAWT, especially the enclosed type with curved inner surface, which increases the value of  $U/U_0$  at  $Z/H = -0.5$  by 69.69%. Meanwhile, the turbine wake deficit in the Z-direction is reduced, and the configuration of the wake profile becomes sharper. This is because a relatively low-pressure region is formed behind the VAWT and the pressure difference increases (see Fig. 13), thereby more wind flows in and the velocity is enlarged correspondingly, which is known as the suction effect [38]. The suction effect gives the basic diffuser the capability to capture and accelerate the wind, and further changes the aerodynamic loads on blade 1, as depicted in Fig. 11. Moreover, the valley value of the wake profile is lower than that of the bare VAWT, which indicates that the wind energy absorption capability in the core region of the VAWT (mid-span section, see Fig. 4(a)) is enhanced. The enclosed type contributes the most to this improvement due to its ideal restriction of the surrounding flow, resulting in a lower wind dissipation rate and a higher power coefficient. Besides, the curved inner surface can produce lower drag force than the flat inner surface, allowing the wind to flow more smoothly through the VAWT. More fluctuations can also be observed in the wake profile near the centerline ( $Z/H = 0$ ), indicating that the basic diffuser will complicate the flow field.

The comparison of the instantaneous three-dimensional vortical structures around the VAWT with and without the basic diffuser at  $\theta = 0^\circ$  are illustrated in Fig. 14. The Q-criterion of  $Q = 300$  is employed to identify and visualize the vortices. The velocity magnitude is used to color the iso-surface. It can be seen from Fig. 14(a) that band-shaped vortices are generated at the tips of blade 1 and blade 2, and are regularly transmitted to the downstream region. Meanwhile, some small-scale vortices gather near

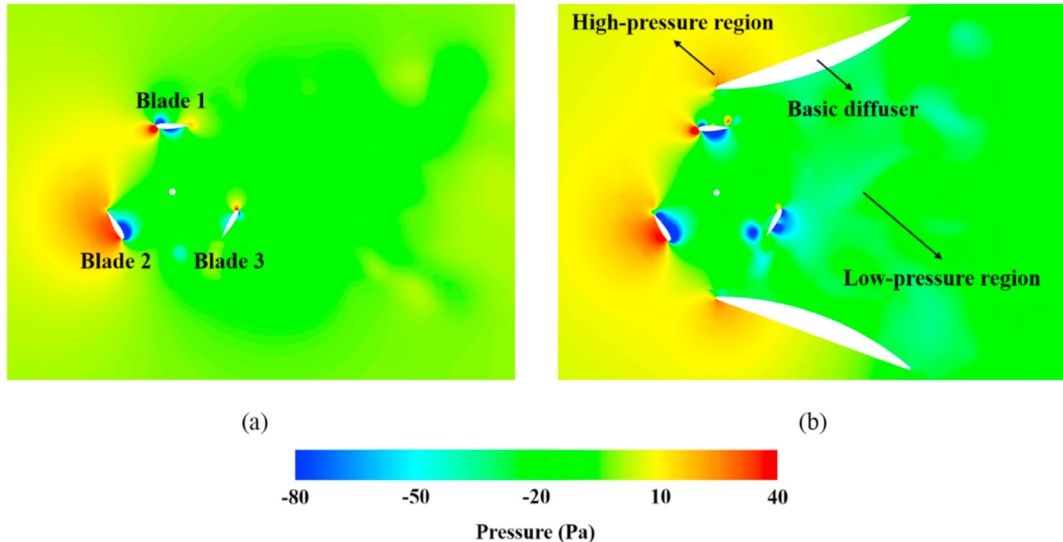


**Fig. 13.** Comparison of the instantaneous pressure distributions in the mid-span section of the VAWT: (a) no diffuser; (b) enclosed type basic diffuser with curved inner surface. (TSR = 1.5).

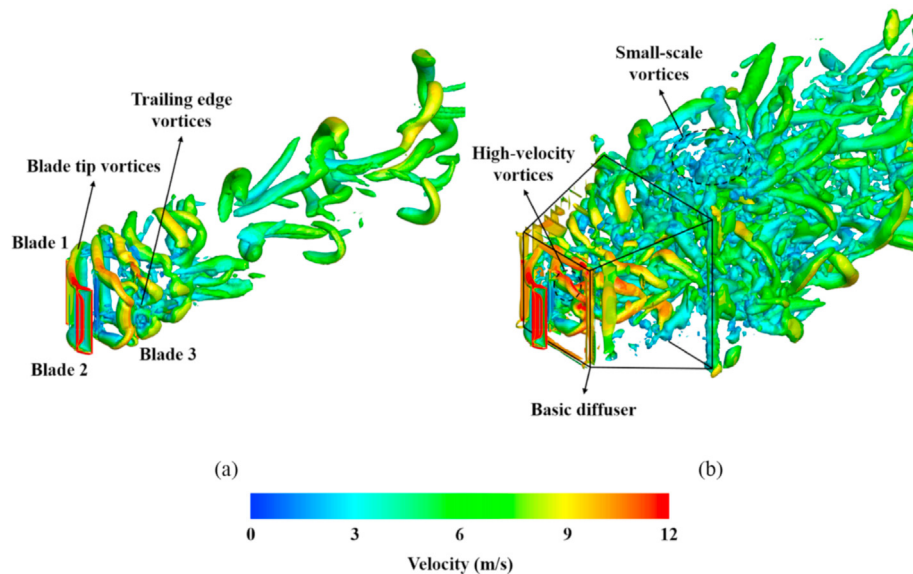


**Fig. 14.** Comparison of the instantaneous three-dimensional vortical structures around the VAWT: (a) no diffuser; (b) enclosed type basic diffuser with curved inner surface. (TSR = 1.5).

the trailing edge of blade 3 and dissipate rapidly. However, the wake field of the VAWT becomes more chaotic when equipped with the basic diffuser, where a large number of small-scale vortices are distributed among the large-scale vortices (see Fig. 14(b)). As a result, the wake profile of the VAWT depicted in Fig. 12 changes significantly because the vortices play an important role in the development of the turbulent flow [63]. Besides, the flow velocity around blade 2 is enlarged and the rotor is surrounded by the high-velocity vortices, resulting in a strong blade-vortex interaction, which ultimately influences the aerodynamic loads of the VAWT.

## 5.2. Effects of the size parameters

In this subsection, a stepwise parametric analysis of the effects of size parameters on the behaviors of the basic diffuser (stage 1) is performed. Based on the previous results, only the enclosed type with curved inner surface is investigated. The projected length  $L_1$  and diffusion angle  $\theta_1$  (see Fig. 4(b)) are taken as the main parameters to be considered. The inlet diameter  $D_{inlet1}$  is kept constant at 1.6D (see Table 2) and the outlet diameter  $D_{outlet1}$  can be calculated using Eq. (9).

Fig. 15 depicts the averaged power coefficients  $C_p$  of the selected VAWT at a series of TSRs for different  $\theta_1$  in the condition of

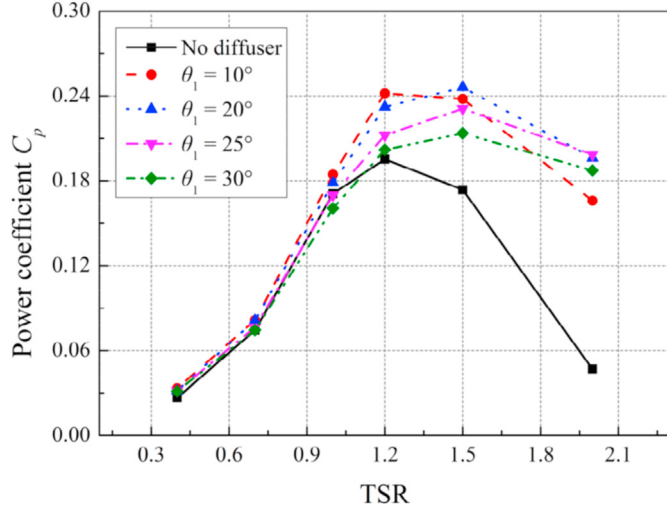


**Fig. 15.** Comparison of the averaged power coefficients of the VAWT for different diffusion angles of the basic diffuser.

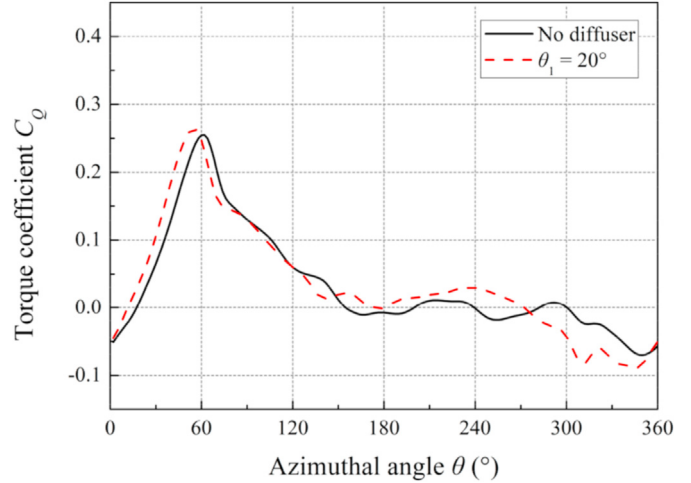


**Fig. 17.** Comparison of the instantaneous torque coefficients of blade 1 with and without the basic diffuser. (TSR = 0.7).

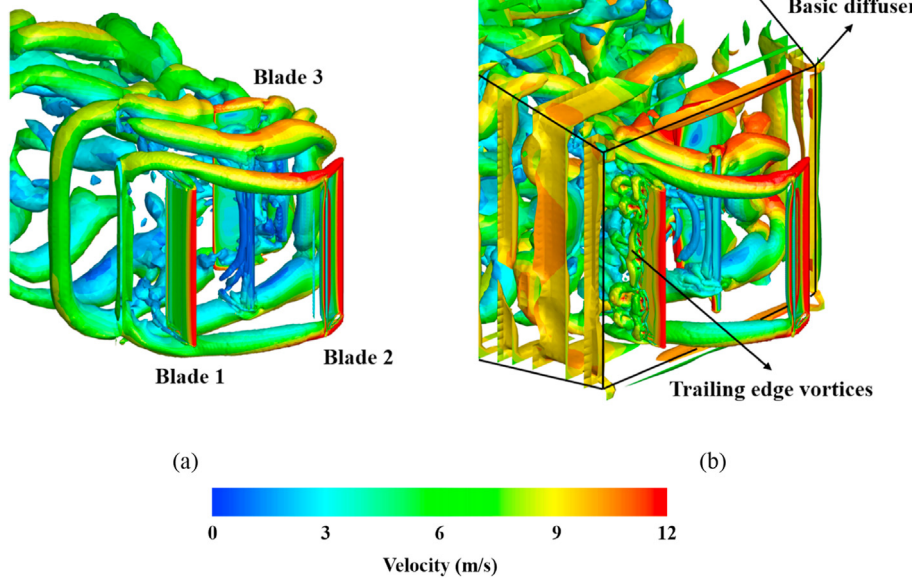


**Fig. 16.** Comparison of the instantaneous three-dimensional vortical structures around blade 1: (a) no diffuser; (b) basic diffuser ( $\theta_1 = 20^\circ$ ). (TSR = 1.5).

$L_1 = 1.5D$ . It can be seen that the basic diffuser can significantly improve the power performance of the VAWT at moderate and high TSRs, while the improvement is not pronounced at low TSRs. Fig. 16 illustrates the comparison of the instantaneous three-dimensional vortical structures around blade 1 with and without the basic diffuser at TSR = 1.5. It can be seen that plenty of small-scale vortices are gathered near the trailing edge of blade 1, which may result in the premature onset of the flow separation and dynamic stall. This is because the enlarged wind velocity caused by the basic diffuser destabilizes the flow field around the VAWT. The above phenomenon will become more intense with decreasing TSR and further weaken the benefits of the basic diffuser. The instantaneous torque coefficients  $C_Q$  of blade 1 within one turbine revolution at TSR = 0.7 depicted in Fig. 17 confirm this point. It can be seen that the improvement of the basic diffuser on the blade torque is

significantly reduced compared to that in Fig. 11, especially in the upwind region, where the relative increase in the peak value of  $C_Q$  drops from 30.83% to 3.57%. Observing the corresponding vorticity distributions illustrated in Fig. 18, it can be found that the vortex shedding at the trailing edge of blade 1 and the vortex attaching on the suction side of blade 3 are enhanced by the basic diffuser, which deteriorates the complex blade aerodynamics at low TSRs and thereby reduces the benefits of the enlarged wind velocity. Besides, the overall capability of the basic diffuser is found to first enhance and then deteriorate as the value of  $\theta_1$  increases, and the TSR required for the VAWT to obtain the peak power output raises from 1.2 to 1.5. The relatively optimal capability is achieved when  $\theta_1 = 20^\circ$ , where  $C_p$  at TSR = 1.5 is increased from 0.1737 to 0.2462. Fig. 19 depicts the instantaneous torque coefficients  $C_Q$  of blade 1 at TSR = 1.5. It shows that among the four diffusion angles, the peak

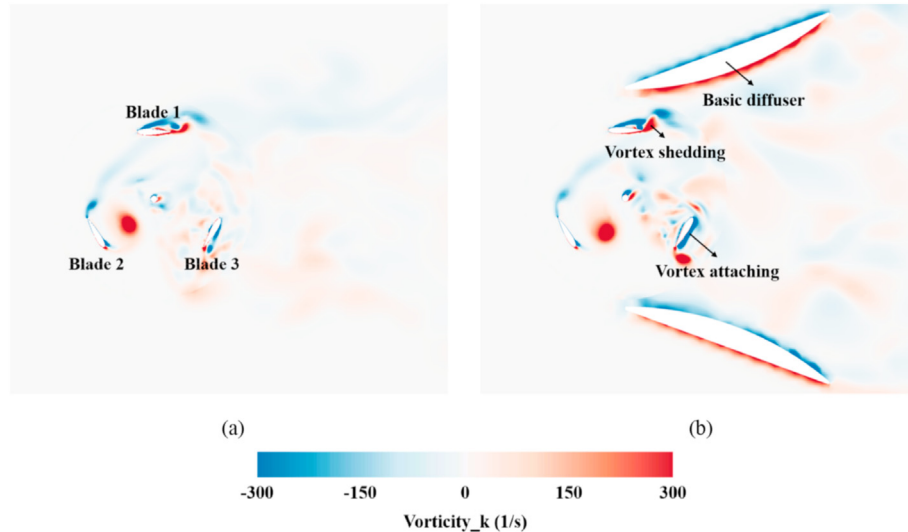


**Fig. 18.** Comparison of the instantaneous vorticity distributions in the middle section of the VAWT: (a) no diffuser; (b) basic diffuser ( $\theta_1 = 20^\circ$ ). (TSR = 0.7).

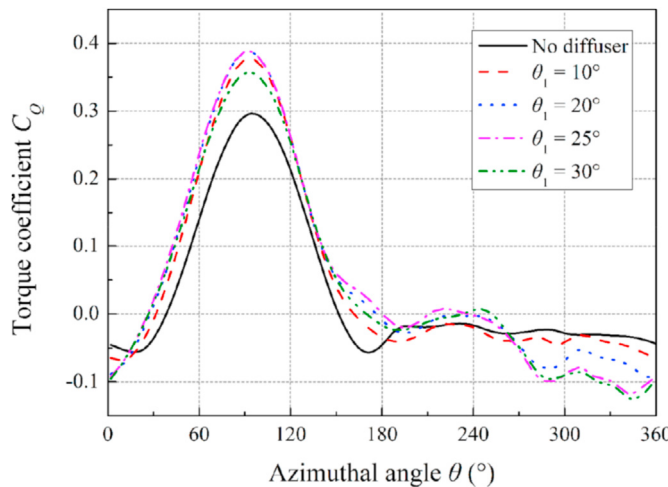


**Fig. 19.** Comparison of the instantaneous torque coefficients of blade 1 for different diffusion angles of the basic diffuser. (TSR = 1.5).

value of  $C_Q$  is the lowest when  $\theta_1 = 30^\circ$ , and the curve presents more fluctuations in the downwind region. This is because an excessive large  $\theta_1$  will complicate and destabilize the flow field inside the basic diffuser to a large extent, thus reducing the wind energy absorption efficiency of the VAWT. The comparison of the averaged normalized wake profiles illustrated in Fig. 20 confirms this point. It can be seen that when  $\theta_1 = 30^\circ$ , the turbine wake deficit at  $Z/H = 0.3$  is substantially reduced compared to that of the other diffusion angles, indicating that the incoming flow is not fully utilized. This phenomenon could also be explained by the findings of Kuang et al. [58]: The combination of high turbulence intensity and high wind velocity would negatively affect the power performance of the VAWT. As to the case of  $\theta_1 = 10^\circ$ , the improvement of the power performance for the VAWT at high TSRs is lower than that of  $\theta_1 = 20^\circ$ . The reason could be that the smaller diffusion angle reduces the pressure difference and thus the flow velocity around

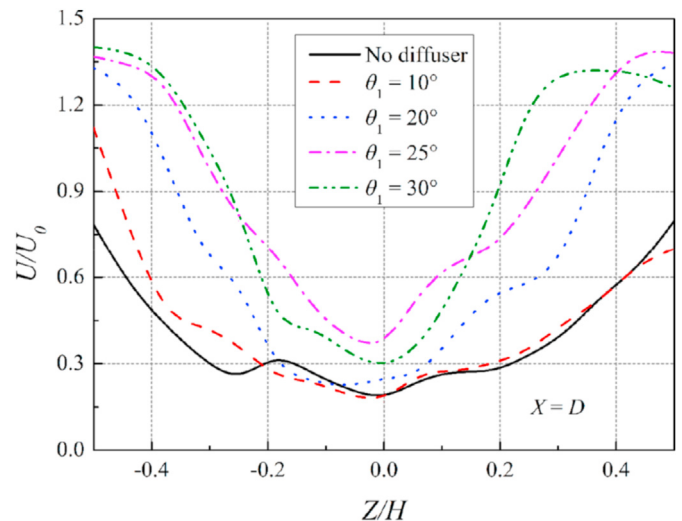


**Fig. 20.** Comparison of the averaged normalized wake profiles of the VAWT in the X-Z plane at the downstream distance of  $X = D$  for different diffusion angles of the basic diffuser. (TSR = 1.5).

the VAWT is decreased. Therefore, the diffusion angle of  $\theta_1 = 20^\circ$  ( $D_{outlet1} = 2.7D$ ) is the relatively optimal choice for the design of the basic diffuser.

The averaged power coefficients  $C_p$  of the VAWT at a series of TSRs for different  $L_1$  in the condition of  $D_{outlet1} = 2.7D$  are depicted in Fig. 21. It can be seen that increasing  $L_1$  is beneficial to improve the power performance of the VAWT, especially for high TSRs. These improvements in  $C_p$  diminish with the growth of  $L_1$  and almost disappear at  $L_1 = 2.5D$ , which indicates that there is a limit to enhance the capability of the basic diffuser by increasing the projected length. Fig. 22 illustrates the comparison of the torque coefficients  $C_Q$  of blade 1 at TSR = 1.5. Since the inlet and outlet diameters of the basic diffuser are fixed, the wind velocities flowing through the VAWT for different  $L_1$  are basically the same, and the difference in the variation trends of  $C_Q$  is small. However, when

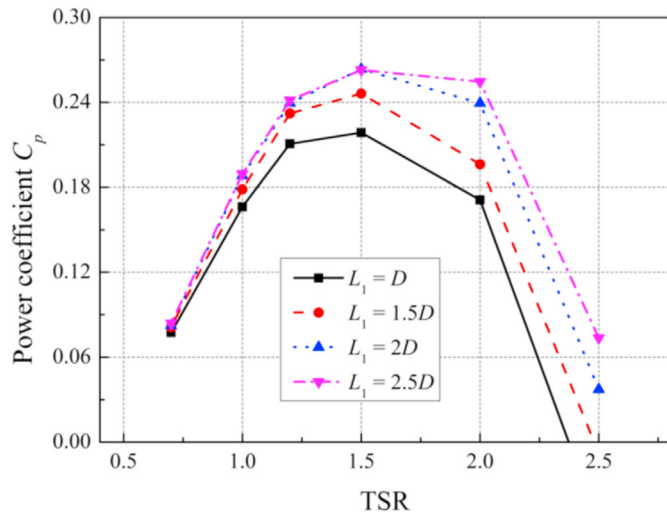


**Fig. 21.** Comparison of the averaged power coefficients of the VAWT for different projected lengths of the basic diffuser.

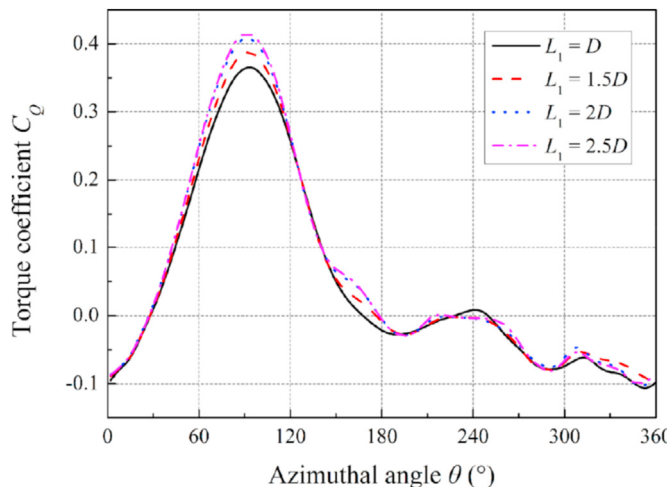


**Fig. 22.** Comparison of the instantaneous torque coefficients of blade 1 for different projected lengths of the basic diffuser. (TSR = 1.5).

$L_1 = D$ , the peak value of  $C_Q$  at  $\theta = 90^\circ$  is noticeably lower than that of the other projected lengths, resulting in a relatively inferior improvement of  $C_p$  depicted in Fig. 21. This phenomenon could be explained by analyzing the averaged wake profiles of the VAWT. It can be seen from Fig. 23 that when  $L_1 = D$ , the normalized wake velocities at  $Z/H < -0.22$  and  $Z/H > 0.19$  exceed 0.9, and the valley value of  $U/U_0$  is the largest, which means that only a small part of the incoming flow is utilized by the VAWT, similar to the case of  $\theta_1 = 30^\circ$ . This is because the shorter projected length prevents the VAWT from fully absorbing the high-velocity wind, thereby negatively affecting its power performance. Besides, the wake profiles of  $L_1 = 2D$  and  $2.5D$  are almost identical, corresponding to the approaching  $C_p$  and  $C_Q$  depicted in Figs. 21 and 22, respectively. Therefore, in consideration of the capability enhancement and manufacturing cost, the suggested projected length of the basic diffuser is  $L_1 = 2D$ .

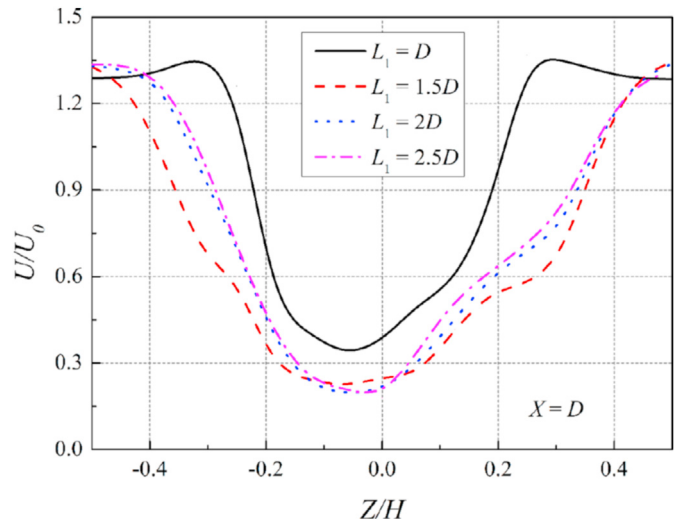


**Fig. 23.** Comparison of the averaged normalized wake profiles of the VAWT in the  $X$ - $Z$  plane at the downstream distance of  $X = D$  for different projected lengths of the basic diffuser. (TSR = 1.5).

### 5.3. Effects of the flange and ejector

The effects of the rear flange (stage 2) and anterior ejector (stage 3) on the behaviors of the basic diffuser are investigated in this subsection, and the size parameters of the two components are optimized in a stepwise manner. The projected length  $L_{2-1}$  and diffusion angle  $\theta_2$  are the main parameters to control the size of the flange. The outlet diameter  $D_{outlet2}$  and projected length  $L_{2-2}$  can be calculated using Eq. (10) and Eq. (12), respectively. According to the results of the parametric analysis in Section 5.2,  $D_{outlet1}$  and  $L_1$  are set to 2.7D and 2D, respectively.

First, the averaged power coefficients  $C_p$  of the selected VAWT at a series of TSRs for different  $\theta_2$  in the condition of  $L_{2-1} = 0.5D$  are depicted in Fig. 24. It can be seen that the flange makes a pronounced contribution to the capability enhancement of the basic diffuser and significantly increases the values of  $C_p$  at  $TSR > 1.2$ . This is because the flange can extend the low-pressure region mentioned in Section 5.1 and generate downstream vortices around the outlet of the basic diffuser (see Fig. 25), which increases the pressure difference. As a result, the suction effect on the incoming flow becomes stronger, and the capability of the basic diffuser to capture and accelerate the wind is enhanced. Besides, the optimal TSR of the VAWT is further increased from 1.5 to 2.0, which means that higher wind velocities require higher angular velocities to accommodate. Moreover, as shown in Fig. 24(a), increasing  $\theta_2$  is found to have small influence on the power performance of the VAWT at  $TSR < 2.0$ . The reason could be that  $L_{2-1}$  is kept constant during the adjustment of  $\theta_2$ , resulting in essentially the same acceleration capability of the basic diffuser. However, the detailed comparison illustrated in Fig. 24(b) suggests that larger  $\theta_2$  contributes more to the values of  $C_p$  at high TSRs, while  $C_p$  benefits more from smaller  $\theta_2$  at low TSRs. For instance, the maximum value of  $C_p$  for  $TSR = 1.5$  is reached at  $\theta_2 = 10^\circ$ , and that for  $TSR = 2.5$  is reached at  $\theta_2 = 15^\circ$ . This indicates that the effects of different  $\theta_2$  on the capability of the basic diffuser cannot be simply measured and the appropriate  $\theta_2$  needs to be determined according to the actual operating conditions of the VAWT. Considering that higher angular

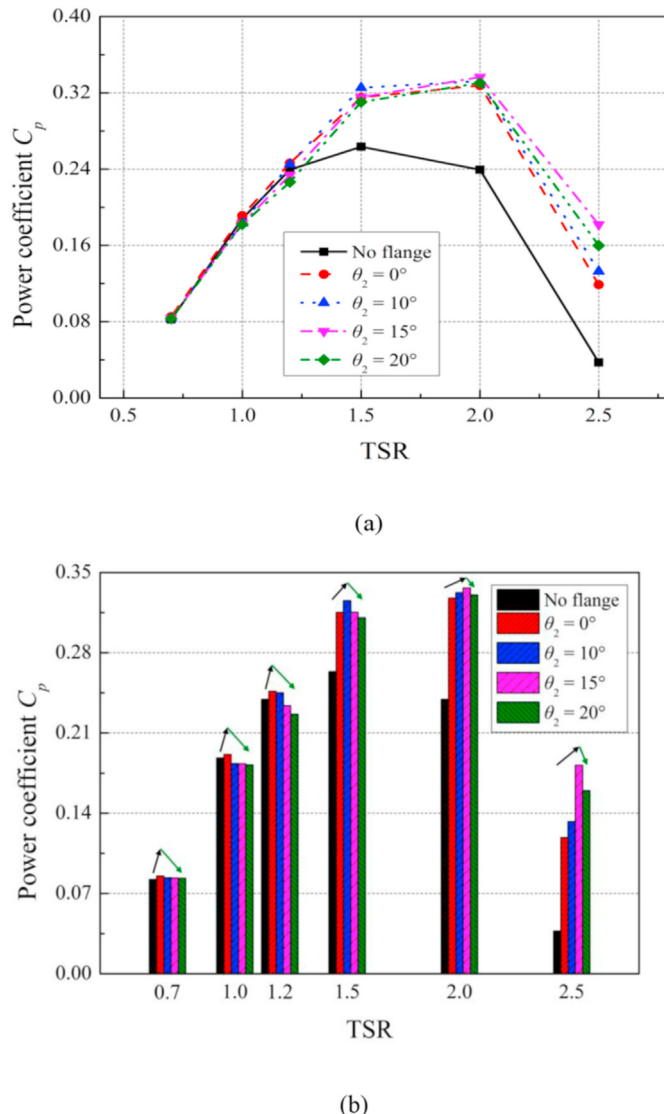


**Fig. 24.** Comparison of the averaged power coefficients of the VAWT for different diffusion angles of the flange: (a) line chart; (b) histogram.

velocity may cause structural vibration problems of the rotor, the diffusion angle of  $\theta_2 = 10^\circ$  ( $L_{2-2} = 0.09D$ ) is suggested for the design of the basic diffuser.

Fig. 26 depicts the averaged power coefficients  $C_p$  of the VAWT at a series of TSRs for different  $L_{2-1}$  in the condition of  $L_{2-2} = 0.09D$ . By increasing  $L_{2-1}$  from  $0.25D$  to  $0.5D$ , the flange provides a more significant enhancement to the capability of the basic diffuser. The values of  $C_p$  at TSR = 1.5, 2.0, and 2.5 are improved by 11.64%, 9.26%, and 61.47%, respectively. This is because the longer  $L_{2-1}$  makes the low-pressure region and downstream vortices larger and stronger, respectively, thereby more wind flows through the basic diffuser and the VAWT can produce more power. However, the power performance of the VAWT deteriorates as  $L_{2-1}$  continues to increase from  $0.5D$  to  $0.75D$ . This phenomenon could be explained by the findings of Kardous et al. [37]: The downstream vortices gradually

move away from the flange along the flow direction with the increase of  $L_{2-1}$ , which is inadequate to enlarge the wind velocity. Therefore, the projected length of  $L_{2-1} = 0.5D$  ( $D_{outlet2} = 3.7D$ ) is the relatively optimal choice for the design of the flange.

Second, similar to the case of the flange, the projected length  $L_3$  and diffusion angle  $\theta_3$  are the main size parameters for the design of the ejector. The outlet diameter  $D_{outlet3}$  can be calculated using Eq. (11). Fig. 27 depicts the power coefficients  $C_p$  of the VAWT at a series of TSRs for different  $\theta_3$  in the condition of  $L_3 = 0.5D$ . Since the ejector can restrain the flow separation at the inlet of the basic diffuser and promote the wind to flow smoothly through the rotor [43], the dynamic stall of the blade with a large variation of AOA is alleviated to a certain extent. As a result, the power performance of the VAWT at low TSRs is found to be significantly improved. Besides, it can be seen that the value of  $C_p$  gradually decreases with increasing  $\theta_3$  when  $TSR \geq 1.2$ , and the optimal TSR of the VAWT drops from 2.0 to 1.5. The reason could be that the ejector with large  $\theta_3$  narrows the high-pressure region in front of the VAWT, thereby the acceleration capability of the basic diffuser is deteriorated. Nevertheless, the diffusion angle of  $\theta_3 = 2.5^\circ$  ( $D_{outlet3} = 1.64D$ ) is found to balance the positive and negative effects of the ejector, resulting in an overall performance improvement of the VAWT.

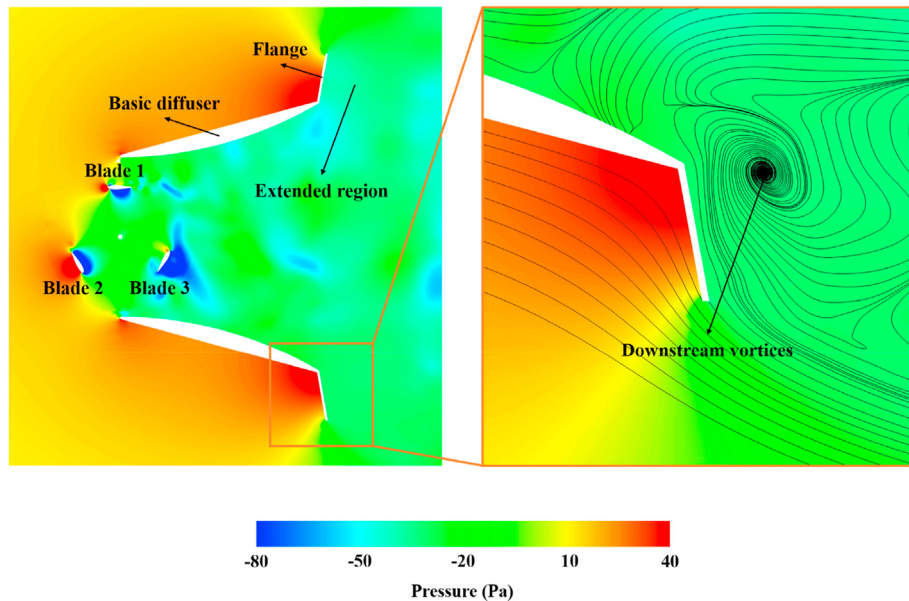
The increasing  $L_3$  also affects the behaviors of the basic diffuser in two aspects. As depicted in Fig. 28, the overall power performance of the VAWT is improved when  $L_3$  increases from  $0.125D$  to  $0.25D$  in the condition of  $D_{outlet3} = 1.64D$ , indicating that the positive effect of the ejector that can draw more wind smoothly into the basic diffuser occupies a domination position. However, the negative effect of reducing the pressure difference is more pronounced when  $L_3 = 0.5D$  and  $0.75D$ . Therefore, the suggested projected length of the ejector is  $L_3 = 0.25D$ .

Table 4 lists the size parameters of the external diffuser system after the parametric analysis. When the selected VAWT is equipped with this wind-capture-accelerate device, its power performance reaches a relative optimum: The value of  $C_p$  at  $TSR = 1.5$  is increased from 0.1737 to 0.3564.

#### 5.4. Analysis of the flow structures

To understand the working mechanism of the external diffuser system at different evolutionary stages, the flow structures around the selected VAWT are analyzed in this subsection. The size parameters of the system are set according to Table 4.

Fig. 29 illustrates the instantaneous vorticity and streamline distributions at different locations in the mid-span section of the VAWT when  $TSR = 1.5$ . It can be seen from Fig. 29(a)-(b)- and (c)-stage 1 that the basic diffuser can significantly change the vorticity field around the rotor, where larger vortices are attached to the blade at  $\theta = 0^\circ$  and  $120^\circ$ , and the flow separation near the trailing edge of the blade becomes more severe at  $\theta = 240^\circ$ . These phenomena are attributed to the high wind velocity and complex flow field caused by the basic diffuser, which are further enhanced by the rear flange: Unstable large-scale vortices are formed on the pressure side of the blade and break up earlier at the trailing edge (see Fig. 29(a)-stage 2), and the location of the severe flow separation is shifted to the leading edge (see Fig. 29(c)-stage 2). As discussed previously in Section 5.3, the intensified flow separation will negatively affect the power performance of the VAWT at low TSRs due to the dynamic stall that may be induced. However, the anterior ejector can alleviate this negative effect where the vorticity



**Fig. 25.** Instantaneous pressure and streamline distributions in the mid-span section of the VAWT ( $\theta_2 = 10^\circ$ ). (TSR = 1.5).

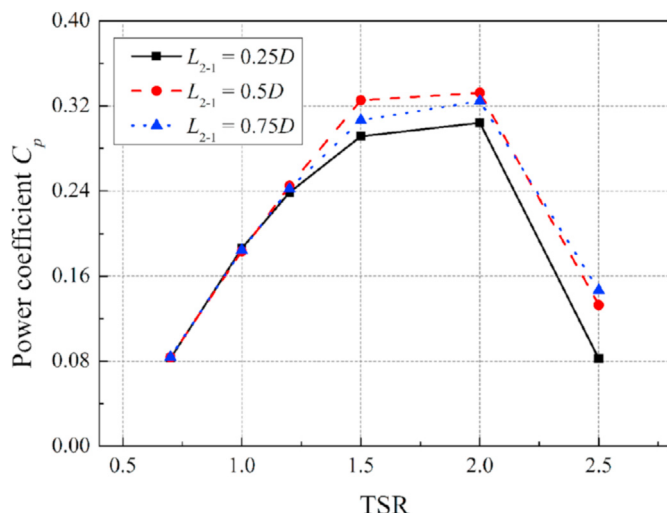


**Fig. 26.** Comparison of the averaged power coefficients of the VAWT for different projected lengths of the flange.

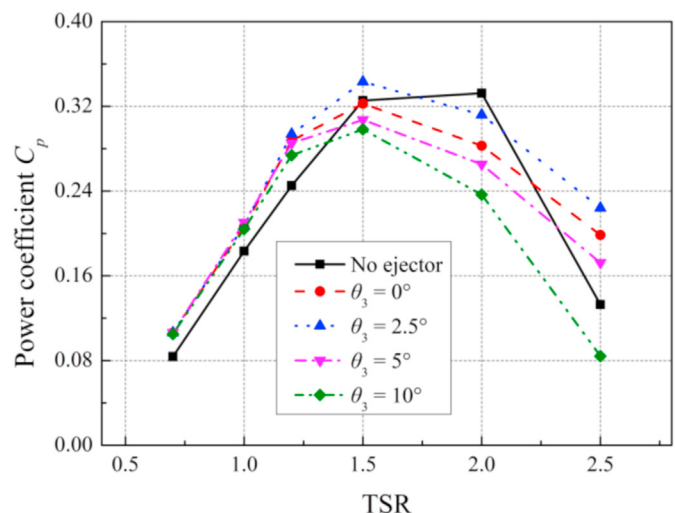


**Fig. 27.** Comparison of the averaged power coefficients of the VAWT for different diffusion angles of the ejector.

field is returned to a relatively stable state (see Fig. 29(a)–and (c)-stage 3). Meanwhile, the strong downstream vortices generated by the flange illustrated in Fig. 29(e)-stage 2 are disappeared as a result of being equipped with the ejector, which will reduce the pressure difference and decrease the wind velocity. Fig. 29(d)-stage 1 and stage 2 indicate that the basic diffuser can reduce the separation of the upstream wind at the inlet and draw more wind flow through the VAWT. Besides, it can be seen from Fig. 29(d)-stage 3 that the ejector provides a transition channel that enables the incoming flow to enter the basic diffuser more smoothly, which corroborates the explanation in Section 5.3.

### 5.5. Application prospect evaluation

Given the doubts of some researchers regarding the feasibility of applying the diffuser-based device to the VAWT, this subsection briefly evaluates the application prospect of the external diffuser system designed in the current study.

In addition to significantly improving the power performance of the VAWT, the unique advantages of the external diffuser system are as follows:

- (1) The safety of the VAWT can be improved by reducing the probability of collision with the external objects, e.g., wind-borne debris and flying birds.

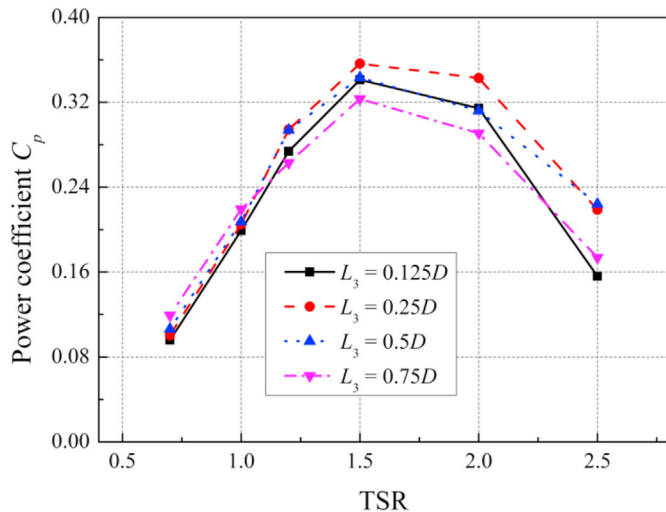


**Fig. 28.** Comparison of the averaged power coefficients of the VAWT for different projected lengths of the ejector.

**Table 4**  
Size parameters of the external diffuser system after the parametric analysis.

Parameter	Symbol	Value
Inlet diameter	$D_{inlet1}$	1.6D
Outlet diameter	$D_{outlet1}$	2.7D
	$D_{outlet2}$	3.7D
Projected length	$D_{outlet3}$	1.64D
	$L_1$	2D
	$L_{2-1}$	0.5D
	$L_{2-2}$	0.09D
	$L_3$	0.25D

- (2) The service life of the VAWT can be extended by reducing the rainfall erosion.
- (3) When encountering the extreme conditions, the public safety risk caused by the falling of the broken blades can be reduced.
- (4) It is possible to use the outer surface of the system for integrated design, e.g., combined with the solar panels [51].

How to alleviate the negative effect on the omnidirectionality of the rotor is addressed as follows:

- (1) Applying to the VAWT located in specific urban areas where the wind direction is relatively homogeneous, e.g., between the buildings and on the rooftops (see Figs. 1 and 30).
- (2) The rear flange can act as a passive yaw system to keep the VAWT facing the incoming flow [36] (see Fig. 31).

Besides, since the system is designed mainly for small-sized VAWTs, the corresponding manufacturing cost is relatively low.

Therefore, the external diffuser system can bring many benefits to the VAWT while alleviating the negative effect on its omnidirectionality, which would have potential applications in specific urban areas.

## 6. Conclusions

In the current study, a wind-capture-accelerate device called external diffuser system is designed to improve the power performance of the VAWT. The basic diffuser, rear flange, and anterior ejector constitute the three evolutionary stages of the system. The three-dimensional IDDES is employed to predict the aerodynamics. The power performance and aerodynamic loads of the VAWT equipped with different types of basic diffusers are compared, and a stepwise parametric analysis of the effects of size parameters is performed. The effects of the flange and ejector on the behaviors of the basic diffuser are investigated. The flow structures around the VAWT are explored and a brief application prospect evaluation is conducted. The main conclusions derived from the results are as follows:

- (1) All types of basic diffusers can significantly improve the power performance of the VAWT, especially the enclosed type with curved inner surface, which increases the power coefficient by 41.74% at TSR = 1.5. The enclosed type is better than the open type due to its ideal restriction of the surrounding flow. The curved inner surface is more effective than the flat inner surface because it can produce lower drag force.
- (2) The suction effect gives the basic diffuser the capability to capture and accelerate the wind. The flow velocity around the VAWT and the aerodynamic loads on the blade are enlarged correspondingly. The considerable enlargement of torque in the upwind region contributes the most to the improvement of the power performance. The increasing peak and valley values of the tangential force are beneficial to the self-starting performance of the VAWT.
- (3) The wake field of the VAWT becomes more chaotic after being equipped with the basic diffuser. The turbine wake deficit is reduced and more fluctuations can be observed in the wake profile near the centerline. The rotor is surrounded by the high-velocity vortices, resulting in a strong blade-vortex interaction, which ultimately influences the aerodynamic loads of the VAWT.
- (4) The flange can further enhance the capability of the basic diffuser by strengthening the suction effect. The ejector sacrifices part of the acceleration capability to promote more wind to flow smoothly through the rotor. As a result, the flow filed around the VAWT is stabilized and the dynamic stall of the blade with a large variation of AOA is alleviated to a certain extent.
- (5) By properly adjusting the projected length and diffusion angle of each component (see Table 4), the relatively optimal capability of the external diffuser system can be achieved.

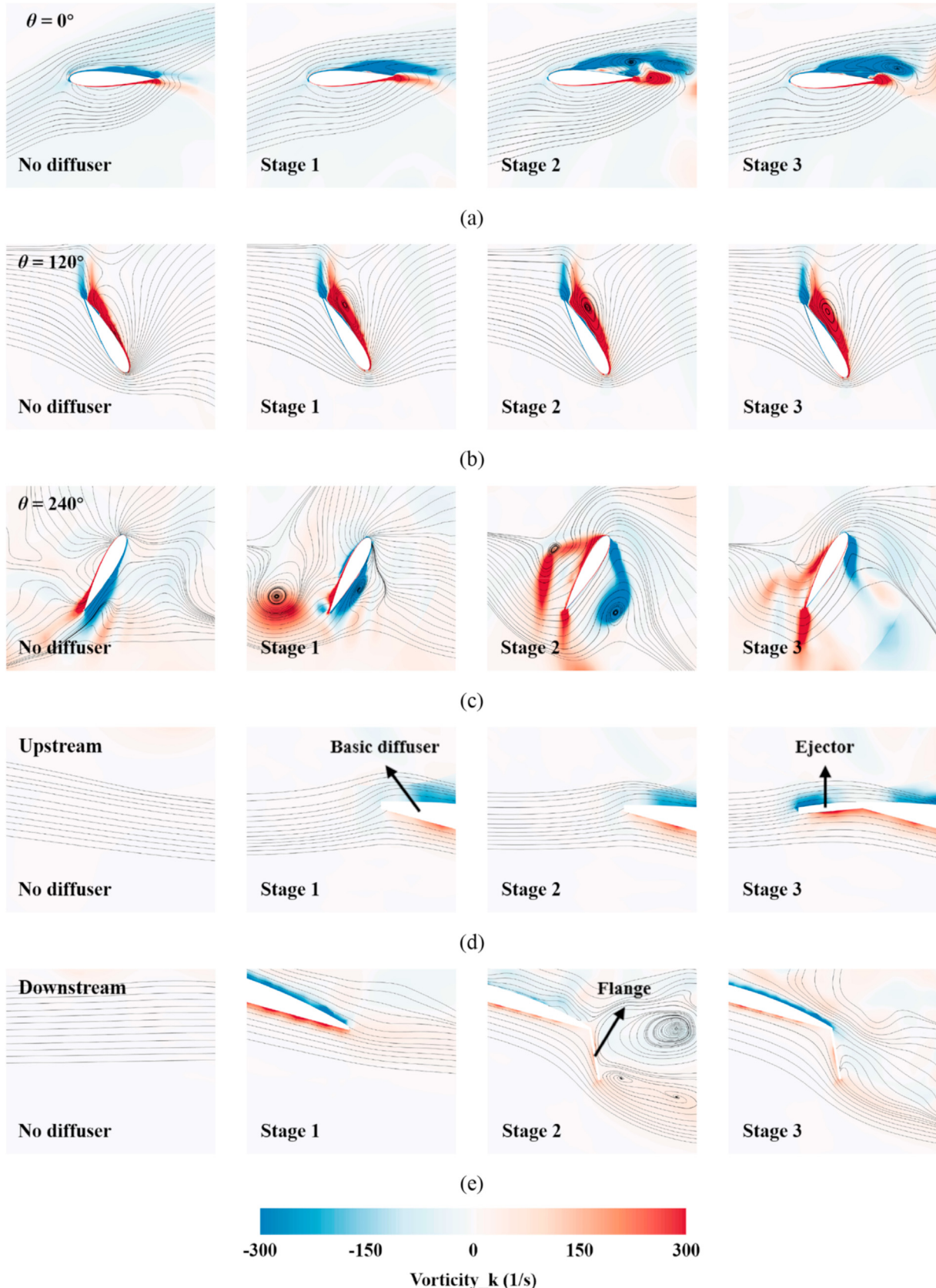


**Fig. 29.** Instantaneous vorticity and streamline distributions at different locations in the mid-span section of the VAWT: (a) blade at  $\theta = 0^\circ$ ; (b) blade at  $\theta = 120^\circ$ ; (c) blade at  $\theta = 240^\circ$ ; (d) upstream; (e) downstream. (TSR = 1.5).

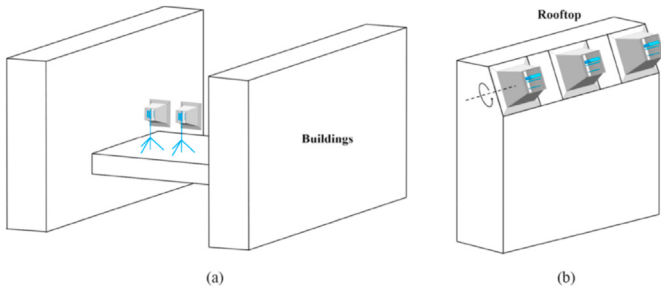


**Fig. 30.** Schematic diagram of the potential application scenarios (not to scale): (a) between the buildings; (b) on the rooftops (Crossflex concept [49]).

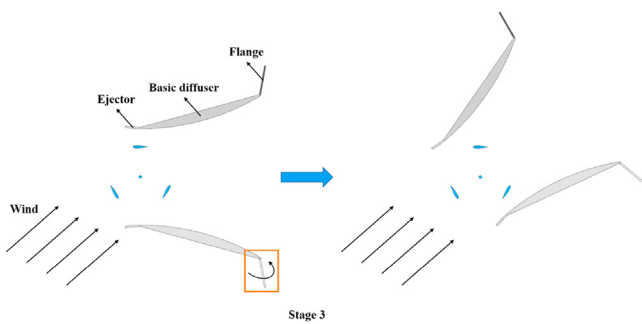


**Fig. 31.** Schematic diagram of the passive yaw mechanism.

The power coefficient of the VAWT at  $TSR = 1.5$  is increased from 0.1737 to 0.3564 after the stepwise parametric analysis. (6) With its unique advantages, certain passive yaw capability, and relatively low manufacturing cost, the external diffuser system can bring many benefits to the VAWT and would have potential applications in specific urban areas.

## Author contribution

**Limin Kuang:** Conceptualization, Methodology, Software, Validation, Formal analysis, Writing - Original Draft, Writing - Review & Editing; **Jie Su:** Methodology, Software, Writing - Review & Editing; **Yaoran Chen:** Writing - Review & Editing; **Zhaolong Han:** Conceptualization, Resources, Writing - Review & Editing, Supervision, Funding acquisition; **Dai Zhou:** Resources, Supervision, Funding acquisition; **Kai Zhang:** Writing - Review & Editing; **Yongsheng Zhao:** Supervision, Funding acquisition; **Yan Bao:** Funding acquisition.

## Declaration of competing interest

The authors declare that they have no known competing financial interests or personal relationships that could have appeared to influence the work reported in this paper.

## Acknowledgments

The financial supports from the Innovation Program of Shanghai Municipal Education Commission (No. 2019-01-07-00-02-E00066), National Natural Science Foundation of China (Nos. 52122110, 52088102, 42076210, 51879160, 51809170, and 11772193), Program for Professor of Special Appointment (Eastern Scholar) at Shanghai Institutions of Higher Learning (No. TP2017013), Program of Shanghai Academic Research Leader (No. 19XD1402000), Shuguang Program of Shanghai Education Development Foundation and Shanghai Municipal Education Commission (No. 19SG10), Oceanic Interdisciplinary Program of Shanghai Jiao Tong University (No. SL2020PT201), and Program for Intergovernmental International S&T Cooperation Projects of Shanghai Municipality (No. 18160744000) are gratefully acknowledged.

## Appendix A. Sensitivity test of the azimuthal increment

A reasonable selection of the azimuthal increment is important for predicting the aerodynamics of the VAWT. In the current study, a sensitivity test of the azimuthal increment is conducted for the selected VAWT with the basic diffuser (stage 1, enclosed type with curved inner surface). The size parameters of the basic diffuser are set according to Table 2. Three azimuthal increments are compared, i.e.,  $\Delta\theta = 1^\circ, 2^\circ$ , and  $4^\circ$ . The instantaneous torque coefficients  $C_Q$  of blade 1 at  $TSR = 1.0, 1.5$ , and  $2.0$  are selected as the comparison objectives. Fig. A1 depicts the instantaneous torque coefficients  $C_Q$  of blade 1 with respect to the azimuthal angle  $\theta$  for different azimuthal increments. It can be seen that the results of  $\Delta\theta = 1^\circ$  and  $\Delta\theta = 2^\circ$  are almost identical, but the variation trend of  $C_Q$  for  $\Delta\theta = 4^\circ$  shows a significant deviation. Besides, the difference between the curves of  $C_Q$  for  $\Delta\theta = 1^\circ$  and  $\Delta\theta = 2^\circ$  becomes slightly more pronounced with the decreasing  $TSR$ , which is consistent with the findings of Rezaeiha et al. [60]. This is because the variation range of the AOA of the blade is relatively large at low  $TSRs$ , where the flow separation on the blade surface will be more intense, and the azimuthal increment is significantly dependent on the flow regime over the blade [60]. Nevertheless, the effect of this small difference on the prediction of the aerodynamics can be neglected. Therefore, in consideration of the computational accuracy and efficiency,  $\Delta\theta = 2^\circ$  is selected for the rest of the simulations.

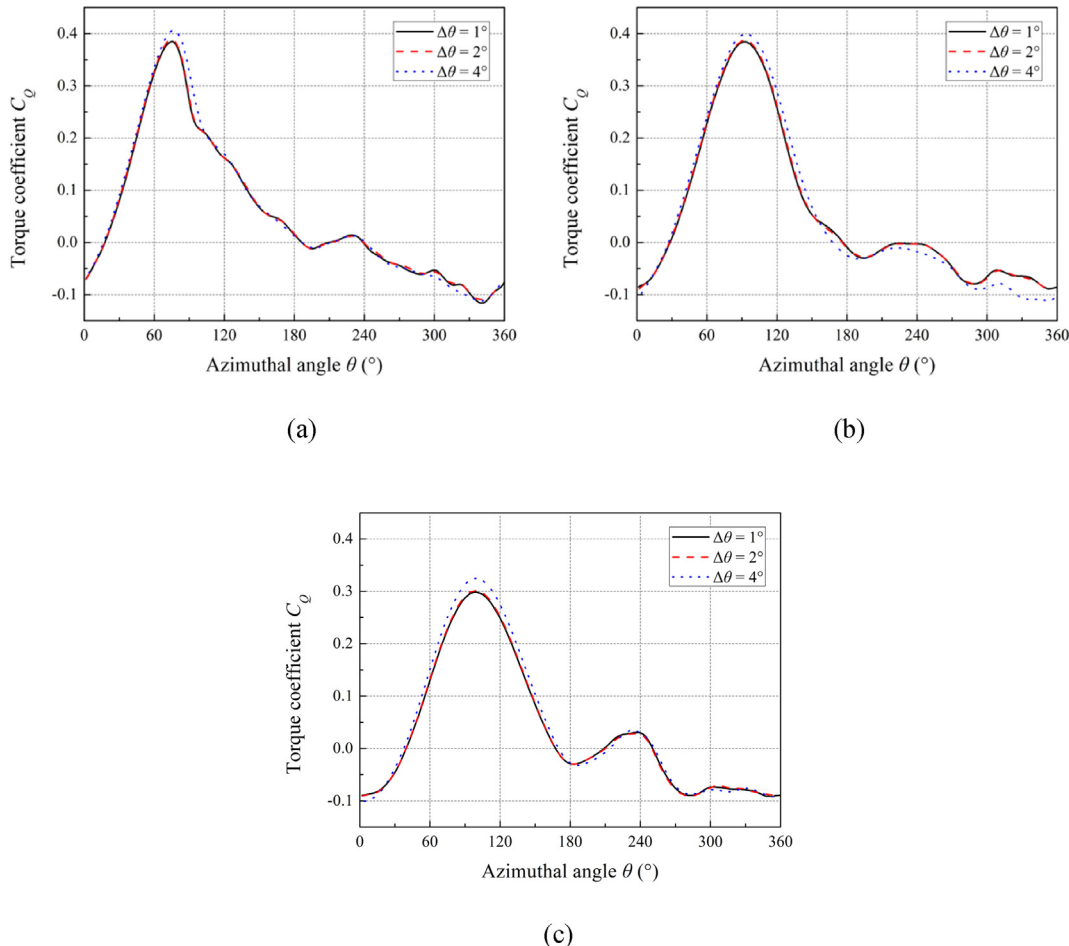


**Fig. A1.** Comparison of the instantaneous torque coefficients of blade 1 for different azimuthal increments: (a) TSR = 1.0; (b) TSR = 1.5; (c) TSR = 2.0.

## References

- [1] Chehouri A, Younes R, Ilinca A, Perron J. Review of performance optimization techniques applied to wind turbines. *Appl Energy* 2015;142:361–88.
- [2] Tummala A, Velamati RK, Sinha DK, Indraja V, Krishna VH. A review on small scale wind turbines. *Renew Sustain Energy Rev* 2016;56:1351–71.
- [3] Ma N, Lei H, Han ZL, Zhou D, Bao Y, Zhang K, Zhou L, Chen CY. Airfoil optimization to improve power performance of a high-solidity vertical axis wind turbine at a moderate tip speed ratio. *Energy* 2018;150:236–52.
- [4] Kuang LM, Su J, Chen YR, Han ZL, Zhou D, Zhao YS, Jiang ZY, Bao Y. Flow characteristics and dynamic responses of a parked straight-bladed vertical axis wind turbine. *Energy Sci. Eng.* 2019;7(5):1767–83.
- [5] Jin X, Zhao GY, Gao KJ, Ju WB. Darrieus vertical axis wind turbine: basic research methods. *Renew Sustain Energy Rev* 2015;42:212–25.
- [6] Li QA, Maeda T, Kamada Y, Murata J, Yamamoto M, Ogasawara T, Shimizu K, Kogaki T. Study on power performance for straight-bladed vertical axis wind turbine by field and wind tunnel test. *Renew Energy* 2016;90:291–300.
- [7] Liu J, Lin H, Zhang J. Review on the technical perspectives and commercial viability of vertical axis wind turbines. *Ocean Eng* 2019;182:608–26.
- [8] Joo S, Choi H, Lee J. Aerodynamic characteristics of two-bladed H-Darrieus at various solidities and rotating speeds. *Energy* 2015;90:439–51.
- [9] Rezaeih A, Montazeri H, Blocken B. Active flow control for power enhancement of vertical axis wind turbines: leading-edge slot suction. *Energy* 2019;189:116131.
- [10] Rezaeih A, Kalkman I, Blocken B. Effect of pitch angle on power performance and aerodynamics of a vertical axis wind turbine. *Appl Energy* 2017;197:132–50.
- [11] Templin R. Aerodynamic performance theory for the NRC vertical-axis wind turbine. In: NASA STI/Recon Technical Report N; 1974. p. 76.
- [12] Paraschivoiu I. Double-multiple streamtube model for studying vertical-axis wind turbines. *J Propul Power* 1988;4(4):370–7.
- [13] Strickland JH, Webster BT, Nguyen T. A vortex model of the darrieus turbine: an analytical and experimental study. *J. Fluids Eng.-Trans. ASME* 1979;101(4):500–5.
- [14] Hirsch IH, Mandal AC. A cascade theory for the aerodynamic performance of Darrieus wind turbines. *Wind Eng* 1987;11(3):164–75.
- [15] Bangga G, Dessoky A, Lutz T, Kramer E. Improved double-multiple-streamtube approach for H-Darrieus vertical axis wind turbine computations. *Energy* 2019;182:673–88.
- [16] Wang LB, Zhang L, Zeng ND. A potential flow 2-D vortex panel model: applications to vertical axis straight blade tidal turbine. *Energy Convers Manag* 2007;48(2):454–61.
- [17] Hand B, Cashman A. Aerodynamic modeling methods for a large-scale vertical axis wind turbine: a comparative study. *Renew Energy* 2018;129:12–31.
- [18] Zhang TT, Elsakka M, Huang W, Wang ZG, Ingham DB, Ma L, Pourkashanian M. Winglet design for vertical axis wind turbines based on a design of experiment and CFD approach. *Energy Convers Manag* 2019;195:712–26.
- [19] Su J, Chen YR, Han ZL, Zhou D, Bao Y, Zhao YS. Investigation of V-shaped blade for the performance improvement of vertical axis wind turbines. *Appl Energy* 2020;260:114326.
- [20] Rezaeih A, Montazeri H, Blocken B. Characterization of aerodynamic performance of vertical axis wind turbines: impact of operational parameters. *Energy Convers Manag* 2018;169:45–77.
- [21] Peng HY, Lam HF. Turbulence effects on the wake characteristics and aerodynamic performance of a straight-bladed vertical axis wind turbine by wind tunnel tests and large eddy simulations. *Energy* 2016;109:557–68.
- [22] Hand B, Kelly G, Cashman A. Numerical simulation of a vertical axis wind turbine airfoil experiencing dynamic stall at high Reynolds numbers. *Comput Fluids* 2017;149:12–30.
- [23] Li Y, Zhao SY, Tagawa K, Feng F. Starting performance effect of a truncated-cone-shaped wind gathering device on small-scale straight-bladed vertical axis wind turbine. *Energy Convers Manag* 2018;167:70–80.
- [24] Wang ZY, Zhuang M. Leading-edge serrations for performance improvement on a vertical-axis wind turbine at low tip-speed-ratios. *Appl Energy* 2017;208:1184–97.
- [25] Xu WH, Li GH, Wang FX, Li Y. High-resolution numerical investigation into the effects of winglet on the aerodynamic performance for a three-dimensional vertical axis wind turbine. *Energy Convers Manag* 2020;205:112333.
- [26] Zhu HT, Hao WX, Li C, Ding QW. Numerical study of effect of solidity on

- vertical axis wind turbine with Gurney flap. *J Wind Eng Ind Aerod* 2019;186: 17–31.
- [27] Zhu HT, Hao WX, Li C, Luo S, Liu QS, Gao C. Effect of geometric parameters of Gurney flap on performance enhancement of straight-bladed vertical axis wind turbine. *Renew Energy* 2021;165:464–80.
- [28] Liu K, Yu ML, Zhu WD. Enhancing wind energy harvesting performance of vertical axis wind turbines with a new hybrid design: a fluid-structure interaction study. *Renew Energy* 2019;140:912–27.
- [29] Poguluri SK, Lee H, Bae YH. An investigation on the aerodynamic performance of a co-axial contra-rotating vertical-axis wind turbine. *Energy* 2021;219: 119547.
- [30] Villeneuve T, Winckelmans G, Dumas G. Increasing the efficiency of vertical-axis turbines through improved blade support structures. *Renew Energy* 2021;169:1386–401.
- [31] Gilbert BL, Oman RA, Foreman KM. Fluid dynamics of diffuser-augmented wind turbines. *J Energy* 1978;2(6):368–74.
- [32] Foreman KM, Gilbert BL, Oman RA. Diffuser augmentation of wind turbines. *Sol Energy* 1978;20(4):305–11.
- [33] Gilbert BL, Foreman KM. Experiments with a diffuser-augmented model wind turbine. *J Energy Resour Technol Trans ASME* 1983;105(1):46–53.
- [34] Igra O. Research and development for shrouded wind turbines. *Energy Convers Manag* 1981;21(1):13–48.
- [35] Bet F, Grassmann H. Upgrading conventional wind turbines. *Renew Energy* 2003;28(1):71–8.
- [36] Ohya Y, Karasudani T, Sakurai A, Abe K, Inoue M. Development of a shrouded wind turbine with a flanged diffuser. *J Wind Eng Ind Aerod* 2008;96(5): 524–39.
- [37] Kardous M, Chaker R, Aloui F, Ben Nasrallah S. On the dependence of an empty flanged diffuser performance on flange height: numerical simulations and PIV visualizations. *Renew Energy* 2013;56:123–8.
- [38] Liu J, Song MX, Chen K, Wu BH, Zhang X. An optimization methodology for wind lens profile using Computational Fluid Dynamics simulation. *Energy* 2016;109:602–11.
- [39] Khamlaj TA, Rumpfkeil MP. Analysis and optimization of ducted wind turbines. *Energy* 2018;162:1234–52.
- [40] Zhu HZ, Sueyoshi M, Hu CH, Yoshida S. A study on a floating type shrouded wind turbine: design, modeling and analysis. *Renew Energy* 2019;134: 1099–113.
- [41] Leloudas SN, Lygidakis GN, Eskantar AI, Nikolos IK. A robust methodology for the design optimization of diffuser augmented wind turbine shrouds. *Renew Energy* 2020;150:722–42.
- [42] Hashem I, Mohamed MH. Aerodynamic performance enhancements of H-rotor Darrieus wind turbine. *Energy* 2018;142:531–45.
- [43] Dessoky A, Bangga G, Lutz T, Kramer E. Aerodynamic and aeroacoustic performance assessment of H-rotor darrieus VAWT equipped with wind-lens technology. *Energy* 2019;175:76–97.
- [44] Watanabe K, Takahashi S, Ohya Y. Application of a diffuser structure to vertical-axis wind turbines. *Energies* 2016;9(6):406.
- [45] Wang XH, Wong KH, Chong WT, Ng JH, Xiang XB, Wang CT. Experimental investigation of a diffuser-integrated vertical axis wind turbine. *IOP Conf Ser: Earth Environ Sci* 2020;463(1):012153.
- [46] Hand B, Cashman A. Conceptual design of a large-scale floating offshore vertical axis wind turbine. *Energy Procedia* 2017;142:83–8.
- [47] Zhu HT, Li C, Hao WX, Ding QW, Yu W. Investigation on aerodynamic characteristics of building augmented vertical axis wind turbine. *J Renew Sustain Energy* 2018;10(5):053302.
- [48] Zhu HT, Hao WX, Li C, Ding QW. Numerical investigation on the effects of different wind directions, solidity, airfoils, and building configurations on the aerodynamic performance of building augmented vertical axis wind turbines. *Int J Green Energy* 2019;16(15):1624–36.
- [49] Sharpe T, Proven G. Crossflex: concept and early development of a true building integrated wind turbine. *Energy Build* 2010;42(12):2365–75.
- [50] Krishnan A, Paraschivoiu M. 3D analysis of building mounted VAWT with diffuser shaped shroud. *Sust Cities Soc* 2016;27:160–6.
- [51] Dilimulati A, Stathopoulos T, Paraschivoiu M. Wind turbine designs for urban applications: a case study of shrouded diffuser casing for turbines. *J Wind Eng Ind Aerod* 2018;175:179–92.
- [52] Zanforlin S, Letizia S. Effects of upstream buildings on the performance of a synergistic roof-and-diffuser augmentation system for cross flow wind turbines. *J Wind Eng Ind Aerod* 2019;184:329–41.
- [53] Alsailani M, Montazeri H, Rezaeiha A. Towards optimal aerodynamic design of wind catchers: impact of geometrical characteristics. *Renew Energy* 2021;168:1344–63.
- [54] Elkhouri M, Kiwata T, Aoun E. Experimental and numerical investigation of a three-dimensional vertical-axis wind turbine with variable-pitch. *J Wind Eng Ind Aerod* 2015;139:111–23.
- [55] Su J, Lei H, Zhou D, Han ZL, Bao Y, Zhu HB. Aerodynamic noise assessment for a vertical axis wind turbine using Improved Delayed Detached Eddy Simulation. *Renew Energy* 2019;141:559–69.
- [56] Shur ML, Spalart PR, Strelets MK, Travin AK. A hybrid RANS-LES approach with delayed-DES and wall-modelled LES capabilities. *Int J Heat Fluid Flow* 2008;29(6):1638–49.
- [57] Lei H, Zhou D, Bao Y, Li Y, Han ZL. Three-dimensional improved delayed detached eddy simulation of a two-bladed vertical axis wind turbine. *Energy Convers Manag* 2017;133:235–48.
- [58] Kuang LM, Lei H, Zhou D, Han ZL, Bao Y, Zhao YS. Numerical investigation of effects of turbulence intensity on aerodynamic performance for straight-bladed vertical-Axis wind turbines. *J Energy Eng ASCE* 2021;147(1):04020087.
- [59] Rezaeiha A, Kalkman I, Blocken B. CFD simulation of a vertical axis wind turbine operating at a moderate tip speed ratio: guidelines for minimum domain size and azimuthal increment. *Renew Energy* 2017;107:373–85.
- [60] Rezaeiha A, Montazeri H, Blocken B. Towards accurate CFD simulations of vertical axis wind turbines at different tip speed ratios and solidities: guidelines for azimuthal increment, domain size and convergence. *Energy Convers Manag* 2018;156:301–16.
- [61] Roache PJ. Perspective: a method for uniform reporting of grid refinement studies. *J. Fluids Eng.-Trans. ASME* 1994;116(3):405–13.
- [62] Roache PJ. Quantification of uncertainty in computational fluid dynamics. *Annu Rev Fluid Mech* 1997;29:123–60.
- [63] Lei H, Zhou D, Bao Y, Chen CY, Ma N, Han ZL. Numerical simulations of the unsteady aerodynamics of a floating vertical axis wind turbine in surge motion. *Energy* 2017;127:1–17.